Late Mesozoic Ore-forming Events in the Ningwu Ore District, Middle-Lower Yangtze River Polymetallic Ore Belt, East China: Evidence from Zircon U-Pb Geochronology and Hf Isotopic Compositions of the Granodioritic Stocks

DUAN Chao[1, *], LI Yanhe[2], HOU Kejun[1, 2], YUAN Shunda[2], LIU Jialin[1] and ZHANG Cheng[1]

1 *State Key laboratory of Geological Processes and Mineral Resources, School of the Earth Sciences and Resources, China University of Geosciences, Beijing 100083, China*
2 *MLR Key Laboratory of Metallogeny and Mineral Assessment, Institute of Mineral Resources, Chinese Academy of Geological Sciences, Beijing 100037, China*

Abstract: Late Mesozoic volcanic-subvolcanic rocks and related iron deposits, known as porphyry iron deposits in China, are widespread in the Ningwu ore district (Cretaceous basin) of the middle–lower Yangtze River polymetallic ore belt, East China. Two types of Late Mesozoic magmatic rocks are exposed: one is dioritic rocks closely related to iron mineralization as the hosted rock, and the other one is granodioritic (-granitic) rocks that cut the ore bodies. To understand the age of the iron mineralization and the ore-forming event, detailed zircon U-Pb dating and Hf isotope measurement were performed on granodioritic stocks in the Washan, Gaocun-Nanshan, Dongshan and Heshangqiao iron deposits in the basin. Four emplacement and crystallization (typically for zircons) ages of granodioritic rocks were measured as 126.1±0.5 Ma, 126.8±0.5 Ma, 127.3±0.5 Ma and 126.3±0.4 Ma, respectively in these four deposits, with the LA-MC-ICP-MS zircon U-Pb method. Based on the above results combined with previous dating, it is inferred that the iron deposits in the Ningwu Cretaceous basin occurred in a very short period of 131–127 Ma. In situ zircon Hf compositions of $\varepsilon_{Hf}(t)$ of the granodiorite are mainly from −3 to −8 and their corresponding $^{176}Hf/^{177}Hf$ ratio are from 0.28245 to 0.28265, indicating similar characteristics of dioritic rocks in the basin. We infer that granodioritic rocks occurring in the Ningwu ore district have an original relationship with dioritic rocks. These new results provide significant evidence for further study of this ore district so as to understand the ore-forming event in the study area.

Key words: Zircon U-Pb age, Hf isotope, porphyry iron deposit, Ningwu ore district, Middle–Lower Yangtze River polymetallic ore belt

1 Introduction

The Middle-Lower Yangtze River polymetallic ore belt (MLYRB) covers an area of ~30000 km^2 and is one of the most important metallogenic belts in East China, comprising seven ore districts, including (from west to east) the Edong, Jiurui, Anqing-Guichi, Tongling, Luzong, Ningwu and Ningzhen (Fig. 1) districts (Chang et al., 1991; Zhai et al., 1992a; Mao et al., 2011). There are more than 200 polymetallic (Cu-Fe-Au, Mo, Zn, Pb, Ag) deposits and widespread magmatic rocks (intrusions, volcanic-subvolcanic rocks) in the Late Mesozoic. The

Ningwu ore district is one of the most important ore districts composed of more than 30 magnetite-apatite deposits, which are known as porphyry iron deposits in China (Fig. 2). There are extensive magmatic rocks comprising volcanic-subvolcanic rocks and granodioritic rocks in the Ningwu ore district. The ages of these igneous rocks and associated metallogenic system have been the major concern among geologists. In the past 10 years, the precise SHRIMP zircon U-Pb, LA-ICP-MS zircon U-Pb and mica Ar-Ar methods were applied to the determination of timing of magmatism and mineralization. Formation ages of four volcanic eruption cycles in the Ningwu ore district were dated at 134.8–126.6 Ma (Zhang
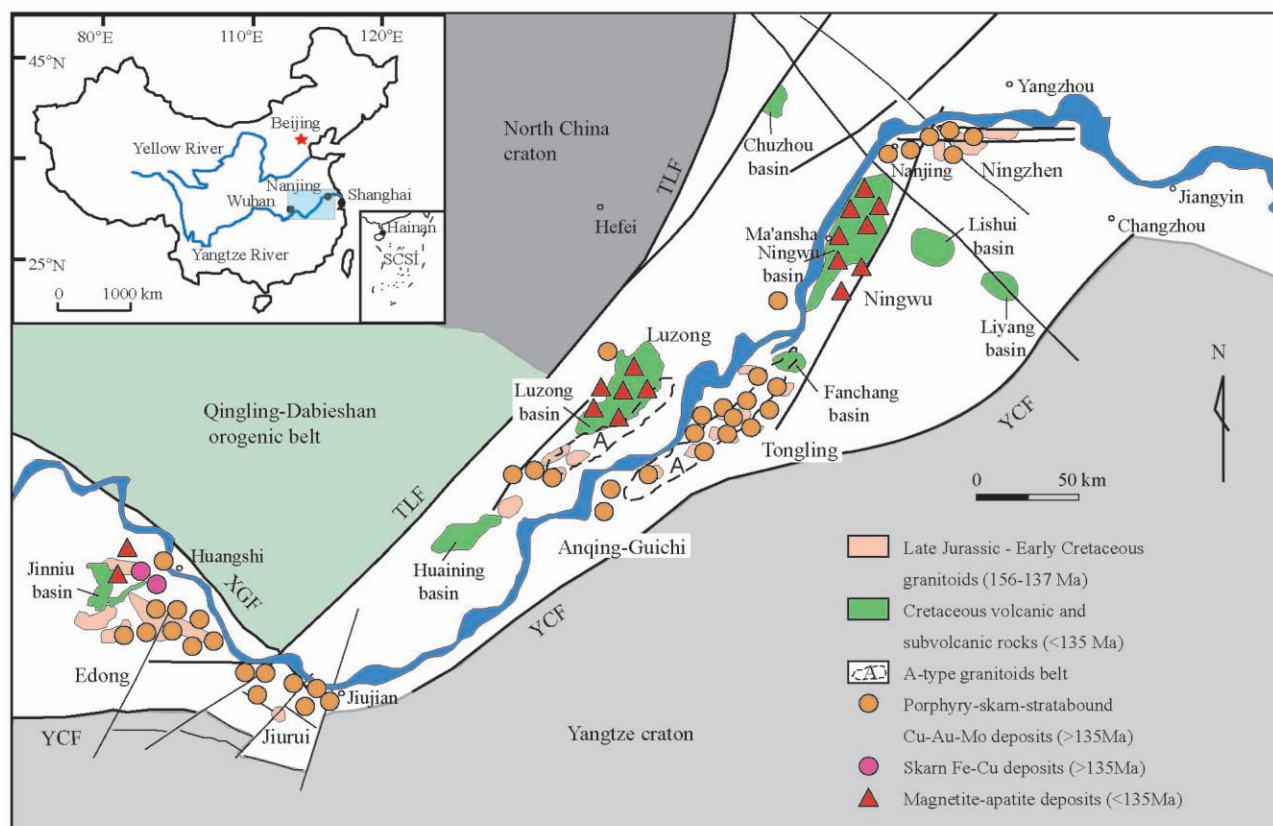

Fig. 1. Geological map of the Middle-Lower Yangtze River polymetallic ore belt, showing the locations of porphyry-skarn-stratabound Cu-Au-Mo-Fe (>135 Ma) and magnetite-apatite deposits (<135 Ma), related granitoids and Cretaceous basins (after Mao et al., 2011). TLF, Tancheng-Lujiang fault; XGF, Xiangfan-Guangji fault; YCF, Yangxing-Changzhou fault.

et al., 2003; Hou and Yuan, 2010; Zhou et al., 2011), and ages of subvolcanic rocks (diorite porphyrite), which are the main wall rock and considered to be related to porphyry iron deposits, were measured at 131.1–128.2 Ma (Fan et al., 2010; Hou and Yuan, 2010; Xue et al., 2010), whereas the range of iron mineralization ages is very broad, 122.9–134.9 Ma (Yu and Mao, 2004; Ma et al., 2006, 2010; Yuan et al., 2010). The ages of iron mineralization throughout the whole period of volcanic activity have been obtained in previous studies, but whether the mineralization continued throughout the whole volcanic period, i.e. all the four volcanic formations, has not been revealed yet.

There are two types of magmatic rocks occurring in iron deposit areas. One is dioritic rocks, which are ore hosted rocks and closely related to iron mineralization, and the other is granodioritic rocks, which occur as stocks and cut ore bodies. To constrain the timing of iron mineralization and better understand the magmatism and iron mineralization, we performed in situ zircon U-Pb and Hf isotopic analyses based on detailed field investigation for granodioritic stocks in the Washan, Nanshan, Dongshan and Heshangqiao iron mines in the middle of the Ningwu ore district.

2 Regional Geological Setting and Geology of Mineral Deposits

The MLYRB, featuring widespread porphyry iron deposits, lies on the northern margin of the Yangtze craton and south of the southeastern margin of the North China craton and the Qinlin-Dabieshan orogenic belt. The Ningwu ore district in the Ningwu volcanic basin is situated in the eastern part of the MLYRB (Fig. 1). It extends from Nanjing (Jiangsu Province) in the northeast to Wuhu (Anhui Province) in the southwest, about 60 km long and 20 km wide with a total area of 1200 km^2 (Fig. 2). The ore district is bounded by the (NNE-striking) Yangtze fault, (NNE-striking) Fangshan-Xiaodanyang fault, (NW-striking) Nanjing-Hushu fault and (E-W-striking) Wuhu fault, and is regarded as an NNE-trending inherited fault-controlled basin (Zhai et al., 1992b).

The Ningwu ore district is characterized by extensive well-developed volcanic-subvolcanic rocks and associated magnetite-apatite deposits, which are considered to be porphyry iron deposits (NRG, 1978). The stratigraphic sequence outcropped in the Ningwu ore district is composed of carbonate, silty and clastic rocks of the Middle-Upper Triassic Qinglong, Zhouchongcun and Huangmaqing
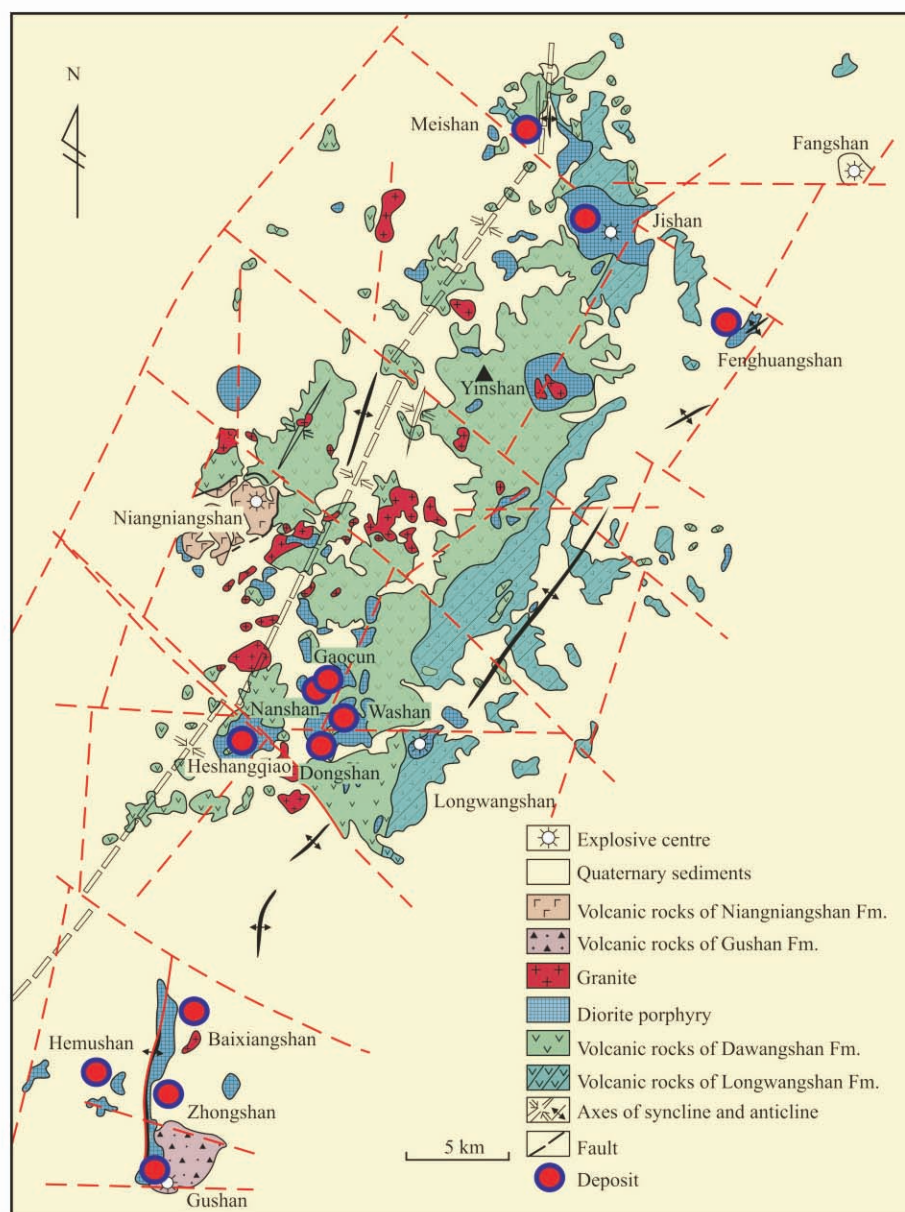
Fig. 2. Geological map showing the distribution of iron deposits of Ningwu ore district (after NRG, 1978).

Formations, and volcanic rock series of the Middle Jurassic Xiangshan and Xihengshan Formations and the Early Cretaceous. At the Late Cretaceous, volcanic rocks were covered by the Pukou and Chishan Formations and Tertiary sedimentary rocks (NRG, 1978; IGCAS, 1987).

Cretaceous volcanic-subvolcanic rocks in the ore district can be divided into four volcanic eruptive-accumulative cycles, i.e. the Longwangshan Formation, the Dawangshan Formation, the Gushan Formation and the Niangniangshan Formation from the bottom up (NRG, 1978) (Fig. 3). Each Formation started with explosive volcanic activity followed by more effusive eruptions, and ended with volcanic sedimentation. The Longwangshan Formation is mainly distributed in the eastern and northern

parts of the basin, covering about 20% of the total area. It consists of sedimentary tuff, silty mudstone and volcanic agglomerate in the lower part, while gibelite, shoshonite and basaltic latite in the upper part. The Dawangshan Formation is the main part of the volcanic rocks, occupying about 75% of the total area. It consists mainly of augite, basaltic latite in the lower part, purple andesite in the middle part, and trachyte and trachytic flood tuff in the upper part. The Gushan and Niangniangshan Formations cover about 5% of the total area, with the former occurring in the south and north parts of the ore district, and composed mainly of andesite, dacite and volcanic breccia, where the latter just occurring near Niangniangshan Mountain in the west, and composed
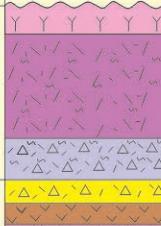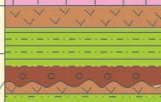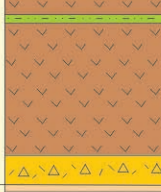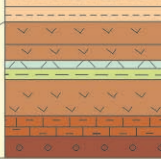
Formation		Thickness (m)	Lithologic column	Age (Ma)		
Niangniangshan	Upper	652		126.6±1.1		
	Lower	230				
Gushan	Upper	185		129.5±0.8	128.2±1.3	
	Lower	102			128.5±1.8	
Dawangshan	Upper	883		132.2±1.6	130.3±0.9	127±3
	Lower	144				
Long-wangshan		513		134.8±1.3		131±4
Reference				Zhou et al., 2011	Hou et al., 2010	Zhang et al., 2003

Fig. 3. Stratigraphic column of the Ningwu volcanic basin with the age of volcanic rocks (Modified after Zhou et al., 2011).

mainly of leucophonolite and hauynite phonolite. These four formations contact one another unconformably (Wang et al., 2001a). Subvolcanic rocks were formed in the late stage of each volcanic cycle and have similar components. The rocks are generally attributed to diorite porphyrite series, i.e. diorite porphyrite, gabbro diorite, gabbro diorite porphyrite, trachyandesitic porphyrite, and andesite porphyrite. Subvolcanic rocks occurring in the Dawangshan cycle is considered to have a close relationship with iron mineralization (NRG, 1978). At the late stage of volcanic activity, a number of granodioritic intrusions occurred in the central part of the area, mostly as small rock bodies (NRG, 1978).

The Ningwu ore district comprises three major orefields: the Meishan, Washan and Zhonggu orefields from north to south (Fig. 2). The Washan, Dongshan, Gaocun (Taocun)-Nanshan, Heshangqiao, Meishan, and Gushan iron deposits are the representatives in these orefields. Mineralization is mostly developed at the apical part of subvolcanic plutons or the surrounding volcanic rocks to form disseminated, massive, breccia, stockwork and hydrothermal vein ore. The ore minerals include chiefly magnetite, hematite, rare pyrite and chalcopyrite, while the major gangue minerals are apatite, albite,

diopside, actinolite, epidote, chlorite and sericite. Hydrothermal alteration is commonly extensive and is characterized by three distinguished alteration zones in space from bottom upwards: 1) alkaline alteration zone, a light colour zone, comprising albite and diopside; 2) dark alteration zone consisting of diopside, actinolite, epidote and chlorite; 3) leucocratic alteration zone made up of quartz, pyrite, hematite, kaolinite, anhydrite and carbonate. Ore bodies mostly occur in secondary alteration zones.

3 Sampling and Analytical Methods

3.1 Sampling and petrology

The samples for dating were collected from four intrusions occurred cutting across the ore bodies in the Washan, the Nanshan, the Dongshan, and the Heshangqiao deposits, respectively. The detailed location and description of samples are listed as follows.

The Washan deposit, characterized by the breccia ore and the hydrothermal vein-type ore, is a large-sized typical porphyry iron deposit. Sample WS-92 was collected from the granodiorite porphyry stock at north of 2# line, −90m in the mine. The stock is very thin with width of about

15m which cut across the western end of the ore body (Fig. 4a). The granodiorite porphyry is characterized by a porphyritic texture with phenocrysts of plagioclase (~30%), quartz (~5%), hornblende and biotite. Pyrite is rare.

The Nanshan deposit, characterized by the disseminated ore and the hydrothermal vein-type ore, is a large-sized iron deposit, 2 km to the north of the Washan deposit. Sample NS-6 was collected from the granodiorite porphyry stock. The stock is thin with width of about 10m, and occurred crossing the north end of the ore body in the Nanshan deposit (Fig. 4b). The rock sample is light meat red with porphyritic structure. Phenocryst is content of plagioclase (~60%), K-Na feldspar (>10%), quartz (15−20%) and hornblende (~5%). Microcrystalline matrixes are mainly plagioclase and quartz. Pyritization frequently occurred.

The Dongshan deposit is a medium-sized iron deposit with high ore grade, and is characterized by the stockwork ore and the hydrothermal vein ore. Sample DSC-11 was collected from the granodiorite porphyry stock at middle of 3# line, −107m in the mine (Fig. 4c). The stock cut across the eastern end of the ore body. It is composed of plagioclase (~25%), albite (~20%), quartz (~5%), hornblende and biotite as phenocrysts, and microcrystalline feldspar and quartz as interstitial matrix.

The Heshangqiao deposit is a large-sized iron deposit started mining recently. The granodiorite porphyry was destructive to the diorite porphyrite which was development of disseminated magnetite (Fig. 4d). Sample HSQ-6 was collected from the drill core of ZKT3908 at −265 m. The granodiorite porphyry is composed of plagioclase (~50%), K-Na feldspar (20−35%), quartz (~15%), and minor hornblende (<3%) and biotite (<5%), with a little chloritization but magnetite mineralization.

3.2 Analytical methods

The samples were first crushed. Then, individual zircons were separated using conventional heavy liquid and magnetic techniques. Representative grains were handpicked under a binocular microscope, mounted in epoxy resin discs, and then polished. Zircons were
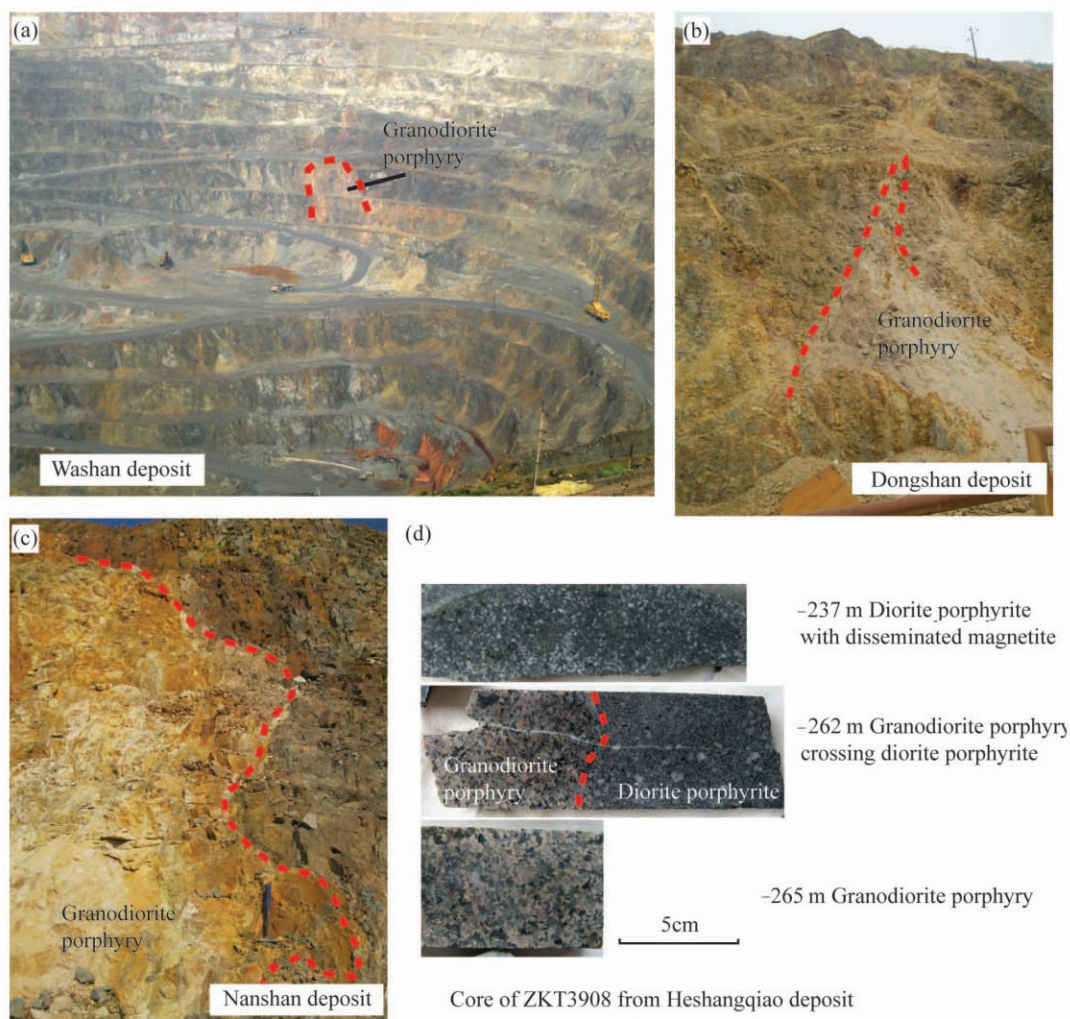
Fig. 4. Positions of sampling.

examined under transmitted and reflected lights, and then imaged by cathode-luminescence (CL) which was obtained using a HITACHI S3000-N microprobe in Institute of Geology, Chinese Academy of Geological Sciences (IGCAS). The zircons, which were euhedral or subhedral, with striped absorption and clear oscillatory zoning rims, were selected for U-Pb and Hf isotope dating.

Zircon U-Pb dating

U-Pb dating analyses were conducted by LA-MC-ICP-MS at the Institute of Mineral Resources, Chinese Academy of Geological Sciences, Beijing. Detailed operating conditions for the laser ablation system and the MC-ICP-MS instrument and data reduction are the same as description by Hou et al. (2009). Laser sampling was performed using a Newwave UP 213 laser ablation system. A Thermo Finnigan Neptune MC-ICP-MS instrument was used to acquire ion-signal intensities. The array of four multi-ion-counters and three faraday cups allow for simultaneous detection of ^{202}Hg(on IC5), ^{204}Hg, ^{204}Pb(on IC4), ^{206}Pb(on IC3), ^{207}Pb(on IC2), ^{208}Pb(on L4), ^{232}Th(on H2), ^{238}U(on H4) ion signals. Helium was applied as a carrier gas. Argon was used as the make-up gas and mixed with the carrier gas via a T-connector before entering the ICP. Each analysis incorporated a background acquisition of approximately 20–30 s (gas blank) followed by 30 s data acquisition from the sample. Off-line raw data selection and integration of background and analytical signals, and time-drift correction and quantitative calibration for U-Pb dating was performed by ICPMSDataCal (Liu et al., 2008). Zircon GJ-1 was used as external standard for U-Pb dating, and was analyzed twice every 5–10 analyses. Time-dependent drifts of U-Th-Pb isotopic ratios were corrected using a linear interpolation (with time) for every 5–10 analyses according to the variations of GJ-1 (i.e., 2 zircons GJ-1 + 5–10 samples + 2 zircons GJ-1) (Liu et al., 2008). Preferred U-Th-Pb isotopic ratios used for GJ-1 are from Jackson et al. (2004). The GJ-1 standard zircon has a crystallization age of 608.5±0.4 Ma, and there is no apparent banding visible in the zircon, which argues for a homo-geneous standard for in-situ analyses (Jackson et al. 2004). Uncertainty of preferred values for the external standard GJ-1 was propagated to the ultimate results of the samples. In all analyzed zircon grains the common Pb correction was not necessary due to the low signal of common ^{204}Pb and high ^{206}Pb/^{204}Pb. U, Th and Pb concentration was calibrated by zircon M-127(with U: 923 ppm; Th: 439 ppm; Th/U: 0.475. Nasdala et al., 2008). Concordia diagrams and weighted mean calculations were made using Isoplot/Ex_ver3. The zircon Plesovice is dated as unknown samples and yielded weighted mean

^{206}Pb/^{238}U age of 337.2±1.7 Ma (2σ, n=8), which is in good agreement with the recommended ^{206}Pb/^{238}U age of 337.13±0.37 Ma (2σ) (Sláma et al., 2008).

In situ zircon Hf isotopic analysis

The zircon Hf analyses of four samples (WS-92, DSC-11, HSQ-5 and NS-6) were done on the same grains as used for U-Pb dating. Zircon Hf isotope analysis was carried out in-situ using a Newwave UP 213 laser-ablation microprobe, attached to a Neptune multi-collector ICP-MS at MRL Key Laboratory of Metallogeny and Mineral Assessment, Institute of Mineral Resources, Chinese Academy of Geological Sciences, Beijing. Instrumental conditions and data acquisition were comprehensively described by Hou et al. (2007) and Wu et al. (2006). A stationary spot was used for the present analyses, with a beam diameter of 55 μm depending on the size of ablated domains. Helium was used as carrier gas to transport the ablated sample from the laser-ablation cell to the ICP-MS torch via a mixing chamber mixed with Argon. In order to correct the isobaric interferences of ^{176}Lu and ^{176}Yb on ^{176}Hf, ^{176}Lu/^{175}Lu =0.02658 and ^{176}Yb/^{173}Yb =0.796218 ratios were determined (Chu et al., 2002). For instrumental mass bias correction Yb isotope ratios were normalized to ^{172}Yb/^{173}Yb of 1.35274 (Chu et al., 2002) and Hf isotope ratios to ^{179}Hf/^{177}Hf of 0.7325 using an exponential law. The mass bias behavior of Lu was assumed to follow that of Yb, mass bias correction protocols details was described as Wu et al. (2006) and Hou et al.(2007). Zircon GJ-1 was used as the reference standard during our routine analyses, with a weighted mean ^{176}Hf/^{177}Hf ratio of 0.282005±0.000016 (2σ, n=16). It is not distinguishable from a weighted mean ^{176}Hf/^{177}Hf ratio of 0.282000±0.000005 (2σ) using a solution analysis method by Morel et al. (2008).

4 Result

4.1 Zircon U-Pb ages

Zircons in the granodiorite porphyry (WS-92) at the Washan iron deposit with 100–150 μm long and 50–100 μm wide, are dominantly euhedral, prismatic, colorless with oscillatory zoning, showed in CL images (Fig. 5). Uranium and thorium concentrations range from 74.4 to 375.6 ppm, and from 74.3 to 284.6 ppm, respectively. Corresponding Th/U ratios are relatively high with ranging from 0.6 to 1.0, indicating their magmatic origin (Belousova et al., 2002; Hoskin and Black, 2000; Wang et al., 2011). 19 analyses of these zircons from the sample WS-92 were obtained and the LA-MC-ICP-MS U-Pb data of these zircons are summarized in Table 1. Of these 19 analyses yielded a weighted average age of 126.1±0.5 Ma
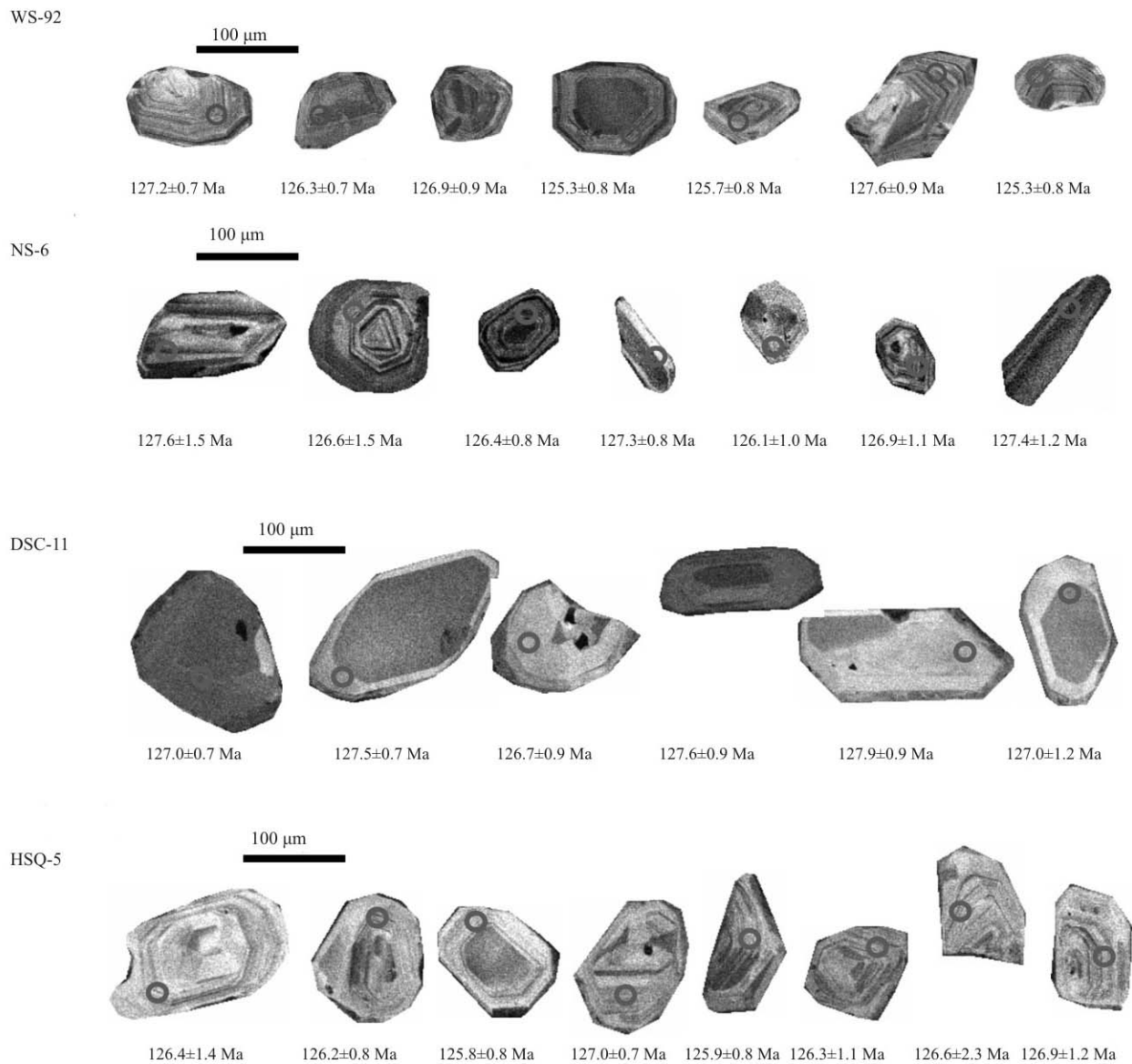
WS-92

127.2±0.7 Ma   126.3±0.7 Ma   126.9±0.9 Ma   125.3±0.8 Ma   125.7±0.8 Ma   127.6±0.9 Ma   125.3±0.8 Ma

NS-6

127.6±1.5 Ma   126.6±1.5 Ma   126.4±0.8 Ma   127.3±0.8 Ma   126.1±1.0 Ma   126.9±1.1 Ma   127.4±1.2 Ma

DSC-11

127.0±0.7 Ma   127.5±0.7 Ma   126.7±0.9 Ma   127.6±0.9 Ma   127.9±0.9 Ma   127.0±1.2 Ma

HSQ-5

126.4±1.4 Ma   126.2±0.8 Ma   125.8±0.8 Ma   127.0±0.7 Ma   125.9±0.8 Ma   126.3±1.1 Ma   126.6±2.3 Ma   126.9±1.2 Ma

Fig. 5. Representative Cathodoluminescence (CL) images of zircons for intrusions with data of zircon U-Pb ages. The circles represent locations of zircon U-Pb and Hf isotopic analyses.

(n=19, MSWD=1.7) (Fig. 6). This age is interpreted as the emplacement age of granodiorite porphyry at the Washan deposit.

Zircons in the granodiorite porphyry (NS-6) at the Nanshan iron deposit are 100–180 μm long and 50–100 μm wide, and are dominantly euhedral, prismatic, and colorless with oscillatory zoning (Fig. 5). Uranium and thorium concentrations range from 63.3 to 276.9 ppm, and from 61.1 to 273.2 ppm, respectively. Corresponding Th/U ratios are relatively high with ranging from 0.6 to 1.3 (Table 1). These indicate a magmatic genesis for the zircons (Belousova et al., 2002; Hoskin and Black, 2000; Wang et al., 2011). 19 analyses of these zircons from the sample NS-6 were obtained and the LA-MC-ICP-MS U-Pb data of these zircons are summarized in Table 1. Of these 19 analyses yielded a weighted average age of

126.8±0.5 Ma (n=19, MSWD=0.8) (Fig. 6). This age is interpreted to be the emplacement age of granodiorite porphyry at the Nanshan deposit.

Zircons in the granodiorite porphyry (DSC-11) at the Dongshan iron deposit are 120–250 μm long and 80–130 μm wide, and are dominantly euhedral, prismatic, and colorless with oscillatory zoning (Fig. 5). Uranium and thorium concentrations range from 26.3 to 160.2 ppm, and from 19.1 to 160.3 ppm, respectively. Corresponding Th/U ratios are relatively high with ranging from 0.6 to 1.1 (Table 1). These indicate a magmatic origin for the zircons (Belousova et al., 2002; Hoskin and Black, 2000; Wang et al., 2011). 19 analyses of these zircons from sample DSC-11 were obtained and the LA-MC-ICP-MS U-Pb data of these zircons are summarized in Table 1. Of these 19 analyses yielded a weighted average age of 127.3±0.5 Ma

Table 1 LA-MC-ICP-MS zircon U-Pb age of the granodiorite porphyries

Sample	Th	U	Th/U	206Pb/238U age (Ma)	1σ	207Pb/206Pb age (Ma)	1σ	207Pb/235U age (Ma)	1σ	206Pb/238U Ratio	1σ	207Pb/206Pb Ratio	1σ	207Pb/235U Ratio	1σ
WS-92															
WS-92-01	74.3	74.4	1.00	127.8	1.0	83.4	32.4	125.9	2.2	0.02002	0.00016	0.04768	0.00076	0.13196	0.00248
WS-92-02	111.2	145.8	0.76	126.5	0.9	168.6	24.1	128.8	1.6	0.01982	0.00014	0.04946	0.00052	0.13526	0.00176
WS-92-03	111.6	171.8	0.65	124.6	0.7	87.1	30.6	122.6	1.2	0.01952	0.00012	0.04776	0.00050	0.12838	0.00136
WS-92-04	165.7	195.3	0.85	127.6	0.8	235.3	63.9	134.0	4.0	0.01998	0.00013	0.05085	0.00132	0.14109	0.00450
WS-92-05	131.6	185.9	0.71	125.7	0.8	127.9	24.1	125.8	1.4	0.01969	0.00013	0.04862	0.00052	0.13185	0.00159
WS-92-06	146.0	217.1	0.67	125.0	0.9	183.4	23.1	128.1	1.2	0.01959	0.00014	0.04977	0.00038	0.13447	0.00138
WS-92-07	284.6	347.6	0.82	124.8	0.8	168.6	25.9	127.2	1.7	0.01955	0.00014	0.04943	0.00055	0.13343	0.00195
WS-92-08	177.5	290.1	0.61	125.3	0.8	187.1	43.5	128.8	2.6	0.01963	0.00012	0.04982	0.00086	0.13522	0.00291
WS-92-09	271.0	342.5	0.79	126.9	0.9	176.0	24.1	129.4	1.5	0.01988	0.00014	0.04958	0.00052	0.13592	0.00172
WS-92-10	142.5	249.6	0.57	124.6	0.9	166.8	27.8	126.4	1.8	0.01952	0.00015	0.04924	0.00060	0.13253	0.00197
WS-92-11	164.9	251.5	0.66	127.4	0.8	183.4	14.8	130.2	1.1	0.01996	0.00013	0.04976	0.00035	0.13680	0.00120
WS-92-12	140.0	204.8	0.68	127.2	0.7	209.3	33.3	131.5	2.0	0.01993	0.00012	0.05032	0.00070	0.13831	0.00227
WS-92-13	116.6	203.2	0.57	126.6	0.7	209.3	18.5	130.9	1.2	0.01983	0.00010	0.05031	0.00041	0.13757	0.00131
WS-92-15	138.7	202.3	0.69	126.3	0.7	168.6	20.4	128.4	1.3	0.01979	0.00011	0.04941	0.00045	0.13483	0.00142
WS-92-16	132.4	231.1	0.57	126.6	0.9	239.0	52.8	133.1	3.8	0.01984	0.00014	0.05094	0.00129	0.14005	0.00431
WS-92-17	143.4	180.4	0.79	125.3	0.8	72.3	31.5	122.6	1.6	0.01962	0.00012	0.04745	0.00064	0.12834	0.00181
WS-92-18	133.0	142.8	0.93	125.3	1.0	109.4	52.8	124.9	2.8	0.01963	0.00016	0.04823	0.00097	0.13085	0.00314
WS-92-19	157.5	240.2	0.66	125.1	0.7	161.2	14.8	127.0	1.0	0.01960	0.00011	0.04928	0.00033	0.13321	0.00111
WS-92-20	276.8	375.6	0.74	127.6	0.9	220.4	14.8	132.6	1.2	0.01999	0.00015	0.05058	0.00031	0.13946	0.00132
NS-6															
NS-6-2	224.6	207.3	1.08	127.6	1.5	166.8	77.8	130.0	5.3	0.01999	0.00024	0.04920	0.00163	0.13663	0.00595
NS-6-3	136.8	216.2	0.63	126.6	1.5	64.9	59.3	123.7	3.4	0.01984	0.00024	0.04732	0.00117	0.12958	0.00380
NS-6-4	96.3	163.0	0.59	126.8	1.2	150.1	70.4	128.7	4.3	0.01987	0.00020	0.04908	0.00145	0.13516	0.00477
NS-6-5	64.0	86.0	0.74	126.1	0.9	116.8	75.9	126.3	5.0	0.01976	0.00015	0.04836	0.00154	0.13243	0.00560
NS-6-6	185.0	270.2	0.68	126.4	0.8	400.1	-366.6	120.3	1.2	0.01980	0.00012	0.04612	0.00039	0.12582	0.00132
NS-6-7	67.0	91.6	0.73	127.6	0.9	101.9	85.2	127.7	6.2	0.01999	0.00014	0.04807	0.00173	0.13407	0.00687
NS-6-8	88.7	122.3	0.73	125.9	1.3	50.1	55.6	123.7	4.4	0.01972	0.00020	0.04703	0.00107	0.12961	0.00488
NS-6-9	61.6	76.0	0.81	125.7	0.8	127.9	44.4	125.9	2.6	0.01969	0.00013	0.04859	0.00092	0.13205	0.00285
NS-6-10	72.7	91.4	0.79	126.1	1.0	87.1	100.0	127.3	8.0	0.01975	0.00016	0.04776	0.00206	0.13358	0.00896
NS-6-11	273.2	211.9	1.29	126.1	1.2	150.1	70.4	129.1	4.9	0.01975	0.00018	0.04908	0.00147	0.13560	0.00543
NS-6-12	157.4	172.5	0.91	125.6	1.0	122.3	27.8	125.6	2.3	0.01967	0.00016	0.04832	0.00060	0.13170	0.00252
NS-6-13	161.0	276.9	0.58	126.9	1.1	127.9	34.3	127.7	2.5	0.01987	0.00017	0.04862	0.00063	0.13401	0.00281
NS-6-14	119.4	148.7	0.80	128.0	0.8	105.6	83.3	128.5	5.9	0.02005	0.00013	0.04814	0.00173	0.13494	0.00660
NS-6-15	70.6	107.0	0.66	126.1	0.9	146.4	77.8	126.8	3.6	0.01975	0.00014	0.04897	0.00162	0.13305	0.00402
NS-6-16	147.9	210.9	0.70	128.6	1.2	79.7	61.1	128.7	4.7	0.02015	0.00019	0.04760	0.00124	0.13514	0.00527
NS-6-17	252.7	200.1	1.26	127.3	0.8	150.1	36.1	128.5	1.9	0.01994	0.00013	0.04904	0.00067	0.13494	0.00218
NS-6-18	61.1	63.3	0.97	126.5	1.3	200.1	55.6	128.9	5.7	0.01982	0.00020	0.04871	0.00116	0.13531	0.00637
NS-6-19	82.7	89.8	0.92	127.8	0.9	166.8	82.4	129.7	5.2	0.02002	0.00014	0.04919	0.00181	0.13629	0.00579
NS-6-20	130.6	118.1	1.11	127.4	1.2	164.9	64.8	130.8	4.5	0.01997	0.00018	0.04936	0.00137	0.13744	0.00505
DSC-11															
DSC-11-1	41.0	53.0	0.77	126.9	0.9	120.5	66.7	126.9	4.1	0.01988	0.00014	0.04847	0.00140	0.13314	0.00457
DSC-11-2	19.1	26.3	0.73	127.4	1.7	13.1	137.0	128.9	14.4	0.01996	0.00027	0.04633	0.00270	0.13539	0.01607
DSC-11-3	33.7	45.0	0.75	127.5	2.9	298.2	159.2	128.8	5.5	0.01998	0.00046	0.05227	0.00364	0.13520	0.00612
DSC-11-4	37.4	50.5	0.74	127.4	0.9	200.1	77.8	127.5	4.0	0.01995	0.00014	0.04872	0.00161	0.13379	0.00448
DSC-11-5	160.3	160.2	1.00	127.0	0.7	101.9	62.0	126.5	4.0	0.01989	0.00011	0.04804	0.00115	0.13266	0.00442
DSC-11-6	65.5	78.8	0.83	127.5	0.7	127.9	38.9	127.0	1.9	0.01997	0.00012	0.04856	0.00078	0.13326	0.00207
DSC-11-7	29.5	45.9	0.64	127.8	1.3	211.2	66.7	131.5	3.3	0.02002	0.00021	0.05020	0.00140	0.13828	0.00371
DSC-11-8	29.1	46.2	0.63	128.3	1.2	139.0	65.7	128.6	3.6	0.02010	0.00019	0.04885	0.00147	0.13497	0.00405
DSC-11-9	53.0	62.5	0.85	128.1	1.2	200.1	73.1	128.2	3.6	0.02008	0.00019	0.04872	0.00143	0.13457	0.00400
DSC-11-10	25.9	42.8	0.60	127.5	1.1	142.7	53.7	127.9	2.7	0.01998	0.00017	0.04886	0.00111	0.13420	0.00306
DSC-11-11	46.4	51.4	0.90	126.7	0.9	127.9	66.7	126.6	3.7	0.01985	0.00015	0.04862	0.00139	0.13283	0.00411
DSC-11-12	55.5	54.2	1.02	127.2	1.0	124.2	84.2	127.3	4.8	0.01993	0.00015	0.04853	0.00165	0.13355	0.00539
DSC-11-13	71.0	72.2	0.98	127.9	0.9	166.8	57.4	128.6	2.9	0.02003	0.00014	0.04918	0.00123	0.13504	0.00322

Table 1 Continued

Sample	Th	U	Th/U	$^{206}Pb/^{238}U$ age (Ma)	1σ	$^{207}Pb/^{206}Pb$ age (Ma)	1σ	$^{207}Pb/^{235}U$ age (Ma)	1σ	$^{206}Pb/^{238}U$ Ratio	1σ	$^{207}Pb/^{206}Pb$ Ratio	1σ	$^{207}Pb/^{235}U$ Ratio	1σ
DSC-11-14	40.5	51.1	0.79	127.6	0.9	142.7	81.5	130.0	6.1	0.02000	0.00015	0.04888	0.00169	0.13656	0.00687
DSC-11-16	29.4	33.8	0.87	127.0	1.2	109.4	111.1	127.0	6.4	0.01989	0.00019	0.04823	0.00228	0.13318	0.00716
DSC-11-17	34.8	54.4	0.64	126.3	0.9	79.7	89.8	124.0	3.1	0.01979	0.00014	0.04758	0.00113	0.12989	0.00345
DSC-11-18	37.5	34.4	1.09	126.9	1.5	57.5	114.8	122.2	5.7	0.01987	0.00023	0.04719	0.00233	0.12788	0.00633
DSC-11-19	22.2	30.5	0.73	127.7	1.0	231.6	65.7	132.8	3.9	0.02001	0.00016	0.05076	0.00152	0.13971	0.00443
DSC-11-20	48.4	66.3	0.73	128.6	1.8	76.0	96.3	128.9	7.2	0.02015	0.00029	0.04754	0.00195	0.13534	0.00801
HSQ-5															
HSQ-5-1	97.3	132.6	0.73	126.4	1.4	13.1	111.1	126.5	11.8	0.01980	0.00022	0.04631	0.00221	0.13268	0.01316
HSQ-5-2	123.6	180.9	0.68	126.6	1.0	20.5	33.3	121.4	1.9	0.01983	0.00016	0.04647	0.00064	0.12699	0.00207
HSQ-5-3	128.8	177.5	0.73	126.2	0.8	20.5	77.8	122.3	5.2	0.01977	0.00013	0.04646	0.00155	0.12804	0.00573
HSQ-5-4	80.5	122.3	0.66	125.7	0.9	20.5	51.8	121.3	3.3	0.01969	0.00014	0.04647	0.00098	0.12694	0.00364
HSQ-5-5	105.4	135.7	0.78	125.8	0.8	101.9	69.4	125.6	4.8	0.01971	0.00012	0.04802	0.00153	0.13165	0.00532
HSQ-5-6	123.9	137.4	0.90	125.8	0.8	77.9	57.4	123.3	3.6	0.01971	0.00012	0.04735	0.00114	0.12914	0.00396
HSQ-5-7	90.2	117.7	0.77	128.3	1.0	5.7	96.3	123.7	6.8	0.02010	0.00015	0.04615	0.00189	0.12951	0.00756
HSQ-5-8	90.4	134.9	0.67	127.0	0.7	87.1	68.5	125.7	4.1	0.01989	0.00012	0.04776	0.00137	0.13180	0.00461
HSQ-5-9	202.9	224.6	0.90	127.2	0.7	400.1	-344.4	121.3	2.8	0.01993	0.00011	0.04606	0.00095	0.12691	0.00313
HSQ-5-10	85.4	132.8	0.64	125.9	0.8	101.9	48.1	124.6	2.5	0.01973	0.00012	0.04806	0.00097	0.13058	0.00278
HSQ-5-11	81.3	119.0	0.68	126.3	1.1	116.8	67.6	127.5	4.5	0.01979	0.00017	0.04836	0.00129	0.13377	0.00503
HSQ-5-13	104.5	128.0	0.82	125.9	0.9	120.5	63.9	125.9	3.5	0.01972	0.00014	0.04843	0.00123	0.13200	0.00386
HSQ-5-14	81.1	111.5	0.73	126.5	1.3	100.1	105.5	131.6	13.0	0.01982	0.00020	0.04789	0.00235	0.13841	0.01459
HSQ-5-15	108.3	143.4	0.76	126.6	2.3	16.8	70.4	126.8	8.3	0.01983	0.00037	0.04633	0.00145	0.13299	0.00926
HSQ-5-16	152.3	187.9	0.81	125.9	1.5	122.3	44.4	128.7	4.3	0.01972	0.00024	0.04831	0.00092	0.13518	0.00480
HSQ-5-17	160.1	150.1	1.07	125.1	0.7	5.7	25.9	119.0	1.3	0.01959	0.00011	0.04617	0.00050	0.12437	0.00139
HSQ-5-18	80.6	110.8	0.73	126.2	0.9	16.8	33.3	120.6	1.9	0.01977	0.00015	0.04634	0.00069	0.12610	0.00211
HSQ-5-19	155.9	244.0	0.64	127.3	1.1	76.0	68.5	126.0	4.8	0.01994	0.00017	0.04754	0.00136	0.13211	0.00535
HSQ-5-20	206.4	214.3	0.96	126.9	1.2	79.7	61.1	125.0	3.9	0.01988	0.00019	0.04758	0.00124	0.13106	0.00430

(n=19, MSWD=0.3) (Fig. 6). This age is interpreted to be the emplacement age of granodiorite porphyry at the Dongshan deposit.

Zircons in the granite (HSQ-5) at the Heshangqiao iron deposit are 120–200 μm long and 80–130 μm wide, and are dominantly euhedral, prismatic, and colorless with oscillatory zoning (Fig. 5). Uranium and thorium concentrations range from 110.8 to 244.0 ppm, and from 80.5 to 206.4 ppm, respectively. Corresponding Th/U ratios are relatively high with ranging from 0.6 to 1.1 (Table 1). These indicate a magmatic origin for the zircons (Belousova et al., 2002; Hoskin and Black, 2000; Wang et al., 2011). 19 analyses of these zircons from sample HSQ-5 were obtained and the LA-MC-ICP-MS U-Pb data of these zircons are summarized in Table 1. Of these 19 analyses yielded a weighted average age of 126.3±0.4Ma (n=19, MSWD=0.7) (Fig. 6). This age is interpreted to be the emplacement age of granite at the Heshangqiao deposit.

4.2 In situ zircon Hf isotope

The zircon grains used for U-Pb dating were large enough to be analyzed for Hf isotope compositions. As expected for zircons, $^{176}Lu/^{177}Hf$ ratios of them are very low, ranging from 0.000485 to 0.003908 (mean value 0.001054). Thus, following the time of zircon crystallization, there was virtually not change in zircon $^{176}Hf/^{177}Hf$ ratios, but a relatively strong change in $\varepsilon_{Hf}(t)$ values due to the increase in chondritic $^{176}Hf/^{177}Hf$ ratios over this period (Siebel and Chen, 2010). This is evident from the differences between the measured and initial $^{176}Hf/^{177}Hf$ values for Late Mesozoic zircons (Table 2).

The zircon grains chosen from the four samples for Hf isotope analysis yield a narrow range of $\varepsilon_{Hf}(t)$ value (−0.4 to −10.4)(Fig. 7). However, there are a little of data beyond of the range. Zircons from the granodiorite porphyry (WS-92) at the Washan mine were analyzed, giving the $\varepsilon_{Hf}(t)$ value range from −2.2 to −6.8. Seventeen of nineteen Hf isotopic spot analyses were obtained for sample NS-6 from the Nanshan mine, yielding the most of $\varepsilon_{Hf}(t)$ values between −0.4 to −7.8. The other two is 7.17 and 1.56. The sample from the Dongshan mine (DSC-11) yields the $\varepsilon_{Hf}(t)$ value, whose range is −1.9 to −10.4. Most of zircon analysis data from sample of the Heshangqiao mine (HSQ-5) shows a similar $\varepsilon_{Hf}(t)$ value range of −3.1 to −6.5 to WS-92, except one (−37.4). All spots have mainly $^{176}Hf/^{177}Hf$ ratios of 0.282401 to 0.282687, yielding two-stage Hf model ages of 1207 Ma to 1844 Ma with a mean age of 1493 Ma, except three grains with $^{176}Hf/^{177}Hf$ ratios of 0.282904, 0.282747 and 0.281637, and two-stage Hf model ages of 724 Ma, 1083 Ma and 3535 Ma respectively.

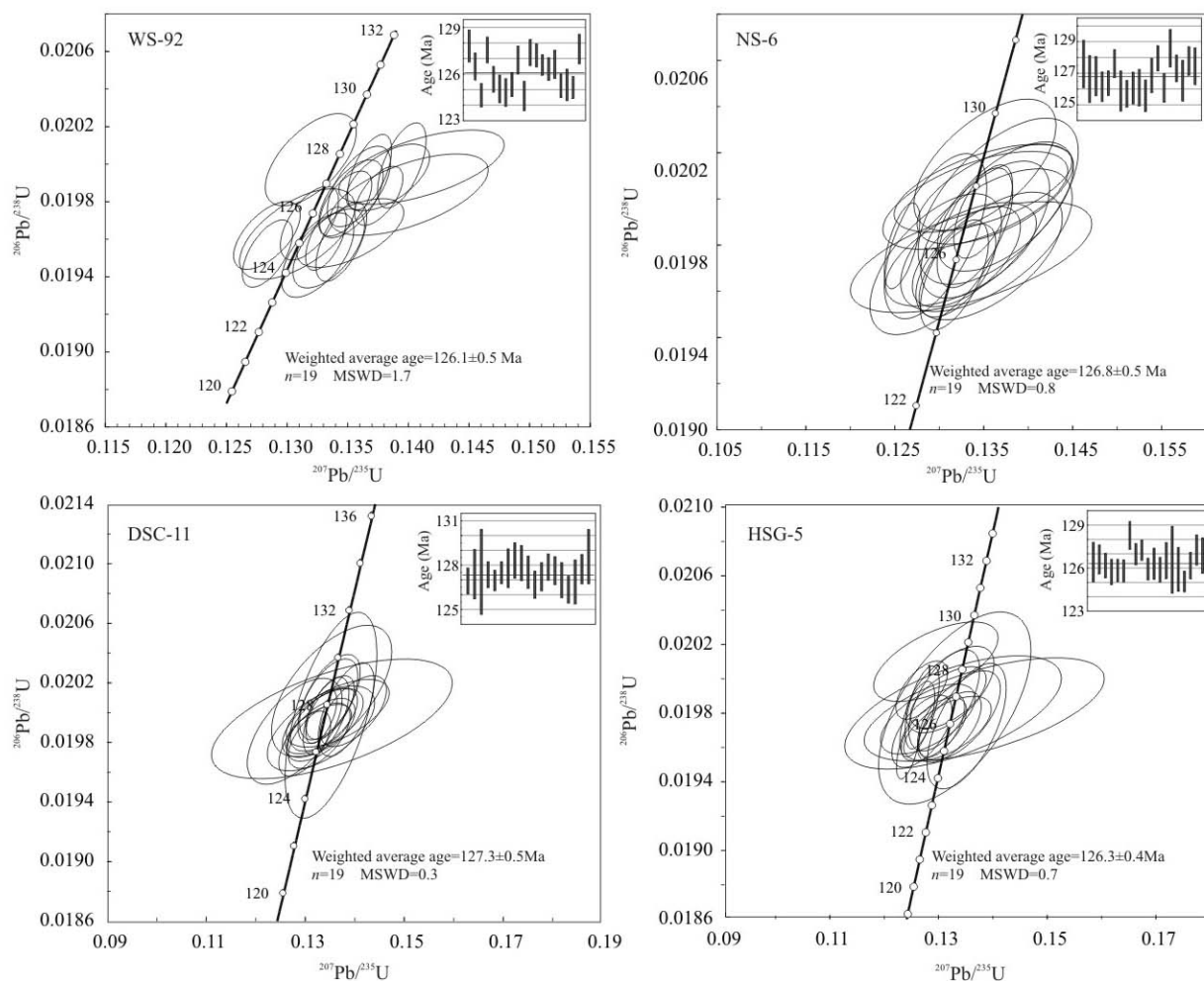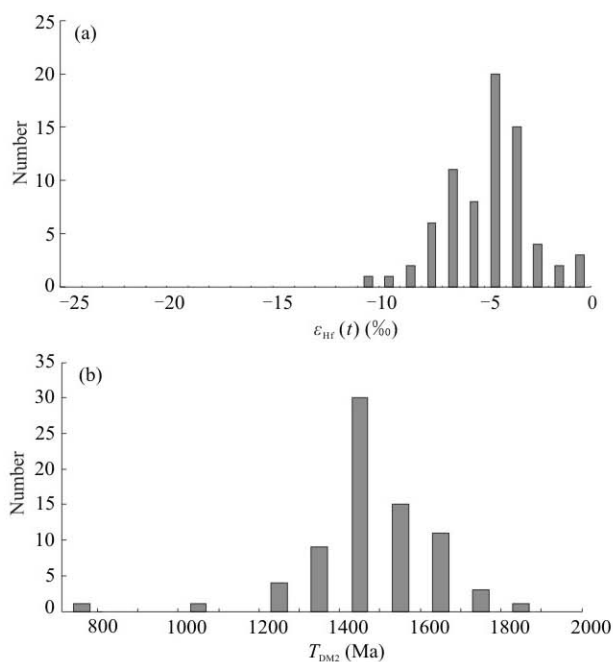Fig. 6. LA-MC-ICP-MS zircon U-Pb concordia diagrams of intrusions.

Fig. 7. Histogram of Zircon εHf(t) values (a) and two-stage model ages (b) of intrusions.

5 Discussion

5.1 Geochronology

The Ningwu volcanic basin is an important ore district in the MLYRB, endowed with numerous large iron deposits and some copper or/and gold deposits. Previous researches have indicated that subvolcanic rocks, especially diorite porphyrite, are associated with the iron deposits (NRG, 1978; Yu and Mao, 2002; Yu et al., 2007, 2008; Hou et al., 2010; Tu et al., 2010).

Timing of these magmatism and mineralization has long been an interesting topic and attracted great attention. In the 1970s and 1980s, the ages of those ore deposits and related granodioritic stocks were yielded by the traditional K-Ar and Rb-Sr isochron methods. The commonly accepted ages are 126.8–125.3 Ma for the Longwangshan Formation, 120.2–121.4 Ma for the Dawangshan Formation, 114.0–109.7 Ma for the Gushan Formation and 105.5–91.0 Ma for the Niangniangshan Formation. The ages of iron mineralization and subvolcanic rocks are 93.1–118.8 Ma and 120.1–125.1 Ma, respectively (NRG, 1978; IGCAS, 1987). These age data provide constraints

on the timing of these magmatism and mineralization in the study area.

In the past ten years, precise SHRIMP zircon U-Pb, LA-ICP-MS zircon U-Pb and Ar-Ar age dating have been applied to constraining the magmatism and mineralization, and a geochron frame of volcanic rocks has been found, as illustrated in Fig. 3. Geochronlogy of subvolcanic rocks (diorite porphyrite) associated with iron deposits (i.e. the host rock) has been systemically measured, and the age range is 131.1–128.2 Ma (Fan et al., 2010; Hou and Yuan, 2010; Xue et al., 2010). However, ages of magnetite-apatite deposits obtained show a wide geochronological range of 122.9–134.9 Ma. Yu and Mao (2004) gained an age of 122.9±0.2 Ma for the Meishan deposit and 124.9±0.3 Ma for the Gaocun (Taocun) deposit with albite Ar-Ar dating, and an age of 126.7±0.2 Ma for the Zhongjiu deposit with phlogopite Ar-Ar dating. Ma et al. (2010) obtained an age of 126–129 Ma for the Dongshan iron deposit with in situ Ar-Ar dating on actinolite. Yuan et al. (2010) obtained ages of 134.9±1.1 Ma, 132.9±1.1 Ma and >128 Ma with Ar-Ar dating on phlogopite for the Baixiangshan, Hemushan and Gaocun (Taocun) iron deposits, respectively. However, whether the mineralization activity (134.9–122.9 Ma) continued throughout the whole volcanic period (134.8–126.6 Ma) has not been revealed yet.

Detailed field investigations conducted by the authors show that disseminated, massive, breccia, stockwork ore and hydrothermal vein ores of iron deposits occur in subvolcanic rocks or surrounding volcanic rocks (the Dawangshan Formation). And the breccia ore consists of a matrix of magnetite with actinolite and minor apatite, hosting diorite porphyrite fragments. The fragments are mostly poorly rounded with alteration in the rim. The above geological facts suggest that iron mineralization occurred later than the cooling of subvolcanic rocks, i.e. 131.1–128.2 Ma (Fan et al., 2010; Hou and Yuan, 2010; Xue et al., 2010). In the mining areas, minor granodioritic rocks occurring as rock stocks, cut across ore bodies without magnetite mineralization (Fig. 4). We collected such rock samples in the Washan, Nanshan, Dongshan and Heshangqiao iron deposits and obtained new zircon LA-MC-ICP-MS U-Pb ages of 127.3–126.1 Ma for granodioritic rocks, which also suggests the lower limit of the timing of mineralization, 127 Ma.

Compared with the ages of volcanic rocks from the four volcanic formations, the data obtained in this study are close to those of the Niangniangshan Formation or/and the Gushan Formation within the error ranges. However, the ages provided by different authors by means of different methods with different experimental errors are slightly different. As stated above, field evidence demonstrates that the diorite porphyrite was formed in the late of Dawangshan Formation. In addition, the NRG (1978) suggested that rubbles of diorite porphyrite and the iron ore in the Gushan Formation in the Zhonggu orefield and Meishan mining area, and the iron mineralization should be earlier than the occurrence of the Gushan Formation. The data we obtained, which are consistent with one another, further confirm this understanding and constrain the iron mineralization in a very short period of 131–127 Ma.

In the late stage of volcanic activity, hydrothermal vein-type copper and/or gold deposits occurred in part of the Ningwu ore district (e.g. Tongjing copper-gold deposit, Dapingshan copper deposit), which are considered to be closely related with the Niangniangshan Formation (NRG, 1978). The ages of the granodioritic stocks are similar to that of the volcanic rocks of the Niangniangshan cycle. Therefore, further research is needed to study the possibility that granodioritic stocks are related to copper and/or gold mineralization.

5.2 Magma source

In this study, the $^{176}Lu/^{177}Hf$ ratios of zircons gained from granodioritic stocks are quite low, which shows that there is little or no accumulation of radiogenic Hf, and the $^{176}Hf/^{177}Hf$ ratios obtained in this study can basically represent the Hf isotopic composition of the magma system during its formation (Wu et al., 2007). As shown in Table 2, Fig. 7 and Fig. 8, the Hf compositions of the late Mesozoic granodioritic stocks crossing the iron ore bodies are characterized by $^{176}Lu/^{177}Hf = 0.000485$–$0.003908$, $^{176}Hf/^{177}Hf=0.281637$–$0.282904$ and $\varepsilon_{Hf}(t)=-37.43$ to 7.17, centered on 0.0008–0.0021, 0.28245–0.28265 and −3 to −8 respectively. The data are clearly different from the composition of the MORB ($^{176}Hf/^{177}Hf$ ratio: Pacific MORB, 0.28313–0.28326; Atlantic MORB, 0.28302–0.28335; Indian MORB, about 0.2832; Patchett and Tatsumoto, 1980; Patchett, 1983; Salters, 1996; Slaters and White, 1998; Chauvel and Blichert-Toft, 2001), as well as those of oceanic basalts worldwide ($\varepsilon_{Hf}(t)>0$) (Salters and Hart, 1991; Hamelin et al., 2010), and are obviously higher than the $\varepsilon_{Hf}(t)$ value of the lower crust in the Yangtze Craton (−62.7, t=126 Ma, 4.0 Ga crust and about −20, t=126 Ma, 1.9 Ga crust, Zhang et al., 2006; Zhang and Zheng, 2007) and lower than the $^{176}Lu/^{177}Hf$ ratio of the crust (average crust: 0.015, Griffin et al., 2002; lower crust: 0.022, and upper crust: 0.0093, Amelin et al., 1999), reflecting that the rocks could not be directly derived by partial melting of the most prominent components at the surface of the Earth, the depleted mantle, the OIB-enriched mantle and the crust. In Fig. 8, the plotted points of the Hf isotopic composition of the

Table 2 In situ zircon Hf isotope compositions of the granodioritic stocks

Sample	t (Ma)	$^{176}Yb/^{177}Hf$	2σ	$^{176}Lu/^{177}Hf$	2σ	$^{176}Hf/^{177}Hf$	2σ	$\varepsilon_{Hf}(0)$	$\varepsilon_{Hf}(t)$	T_{DM1} (Ma)	T_{DM2} (Ma)	$f_{Lu/Hf}$
WS-92-1	127.8	0.072729	0.000264	0.001116	0.000011	0.282502	0.000016	−9.53	−6.82	1063	1617	−0.97
WS-92-2	126.5	0.115177	0.003166	0.001604	0.000041	0.282635	0.000022	−4.86	−2.21	888	1323	−0.95
WS-92-3	124.6	0.081302	0.000282	0.001307	0.000003	0.282570	0.000020	−7.14	−4.52	973	1468	−0.96
WS-92-4	127.6	0.074687	0.000490	0.001266	0.000009	0.282526	0.000020	−8.70	−6.00	1034	1565	−0.96
WS-92-5	125.7	0.083864	0.001112	0.001699	0.000031	0.282595	0.000019	−6.26	−3.64	947	1413	−0.95
WS-92-6	125.0	0.091571	0.001240	0.001538	0.000018	0.282586	0.000017	−6.59	−3.98	956	1434	−0.95
WS-92-7	124.8	0.069093	0.000847	0.001178	0.000011	0.282582	0.000017	−6.71	−4.07	952	1440	−0.96
WS-92-8	125.3	0.102590	0.000306	0.001807	0.000006	0.282574	0.000019	−6.99	−4.39	980	1461	−0.95
WS-92-9	126.9	0.084486	0.000604	0.001491	0.000009	0.282555	0.000018	−7.66	−5.00	998	1501	−0.96
WS-92-10	124.6	0.051786	0.000449	0.000891	0.000007	0.282545	0.000017	−8.04	−5.38	997	1523	−0.97
WS-92-11	127.4	0.063532	0.000470	0.001306	0.000005	0.282570	0.000014	−7.14	−4.45	972	1466	−0.96
WS-92-12	127.2	0.049542	0.000241	0.000952	0.000015	0.282557	0.000017	−7.62	−4.91	982	1495	−0.97
WS-92-13	126.6	0.058599	0.000334	0.001085	0.000004	0.282594	0.000019	−6.29	−3.61	933	1412	−0.97
WS-92-15	126.3	0.084359	0.000632	0.001603	0.000009	0.282571	0.000018	−7.11	−4.47	979	1467	−0.95
WS-92-16	126.6	0.093598	0.000385	0.001664	0.000009	0.282634	0.000018	−4.87	−2.23	890	1324	−0.95
WS-92-17	125.3	0.073109	0.001028	0.001278	0.000017	0.282593	0.000018	−6.34	−3.70	940	1417	−0.96
WS-92-18	125.3	0.085523	0.000153	0.001469	0.000002	0.282600	0.000019	−6.07	−3.44	934	1401	−0.96
WS-92-19	125.1	0.066205	0.001019	0.001135	0.000015	0.282541	0.000018	−8.16	−5.51	1009	1531	−0.97
WS-92-20	127.6	0.075886	0.001168	0.001371	0.000020	0.282556	0.000018	−7.63	−4.95	994	1498	−0.96
NS-6-2	127.6	0.116202	0.004428	0.001893	0.000093	0.282687	0.000020	−3.02	−0.38	820	1207	−0.94
NS-6-3	126.6	0.073898	0.001726	0.001419	0.000054	0.282539	0.000019	−8.25	−5.59	1020	1538	−0.96
NS-6-4	126.8	0.071679	0.000359	0.001285	0.000003	0.282476	0.000018	−10.48	−7.80	1105	1678	−0.96
NS-6-5	126.1	0.090751	0.001252	0.001703	0.000020	0.282670	0.000018	−3.62	−0.99	840	1245	−0.95
NS-6-6	126.4	0.090992	0.000596	0.001566	0.000007	0.282587	0.000022	−6.55	−3.91	955	1431	−0.95
NS-6-7	127.6	0.069043	0.001305	0.001145	0.000019	0.282584	0.000026	−6.65	−3.95	949	1435	−0.97
NS-6-8	125.9	0.098499	0.000731	0.001553	0.000014	0.282589	0.000021	−6.47	−3.83	952	1426	−0.95
NS-6-9	125.7	0.091282	0.000989	0.001454	0.000013	0.282602	0.000023	−6.00	−3.36	930	1396	−0.96
NS-6-10	126.1	0.079755	0.000939	0.001427	0.000021	0.282625	0.000021	−5.21	−2.56	898	1345	−0.96
NS-6-11	126.1	0.219897	0.003902	0.003180	0.000053	0.282904	0.000027	4.66	7.17	524	724	−0.90
NS-6-12	125.6	0.201006	0.003296	0.003908	0.000045	0.282747	0.000028	−0.88	1.55	775	1083	−0.88
NS-6-13	126.9	0.096178	0.000909	0.001629	0.000010	0.282508	0.000020	−9.32	−6.67	1069	1607	−0.95
NS-6-14	128.0	0.050038	0.000232	0.001016	0.000005	0.282605	0.000016	−5.91	−3.19	916	1386	−0.97
NS-6-15	126.1	0.112771	0.001246	0.002111	0.000035	0.282624	0.000016	−5.22	−2.63	915	1349	−0.94
NS-6-16	128.6	0.067368	0.001186	0.001410	0.000027	0.282515	0.000017	−9.10	−6.40	1054	1591	−0.96
NS-6-17	127.3	0.171627	0.000711	0.003430	0.000010	0.282657	0.000025	−4.06	−1.56	900	1282	−0.90
NS-6-18	126.5	0.061183	0.000557	0.001055	0.000010	0.282523	0.000020	−8.80	−6.11	1032	1571	−0.97
NS-6-19	127.8	0.100281	0.000330	0.001561	0.000003	0.282559	0.000022	−7.54	−4.87	995	1493	−0.95
NS-6-20	127.4	0.104088	0.001036	0.001622	0.000031	0.282675	0.000021	−3.43	−0.77	831	1232	−0.95
DSC-11-1	126.9	0.037824	0.000424	0.000598	0.000005	0.282489	0.000019	−10.01	−7.28	1067	1646	−0.98
DSC-11-2	127.4	0.063352	0.000508	0.000981	0.000009	0.282510	0.000018	−9.28	−6.57	1049	1600	−0.97
DSC-11-3	127.5	0.055924	0.000278	0.000851	0.000003	0.282480	0.000019	−10.34	−7.61	1087	1667	−0.97
DSC-11-4	127.4	0.057248	0.000211	0.000917	0.000003	0.282523	0.000015	−8.80	−6.08	1028	1570	−0.97
DSC-11-5	127.0	0.162684	0.000269	0.002537	0.000009	0.282647	0.000020	−4.42	−1.85	893	1300	−0.92
DSC-11-6	127.5	0.071082	0.000608	0.001060	0.000006	0.282523	0.000018	−8.81	−6.10	1032	1571	−0.97
DSC-11-7	127.8	0.074300	0.000546	0.001087	0.000004	0.282552	0.000016	−7.78	−5.07	992	1506	−0.97
DSC-11-8	128.3	0.119490	0.005976	0.001754	0.000091	0.282570	0.000022	−7.14	−4.47	984	1468	−0.95
DSC-11-9	128.1	0.041737	0.000511	0.000598	0.000005	0.282474	0.000019	−10.54	−7.77	1088	1678	−0.98
DSC-11-10	127.5	0.042027	0.000206	0.000629	0.000002	0.282458	0.000020	−11.09	−8.35	1111	1714	−0.98
DSC-11-11	126.7	0.063600	0.000493	0.000947	0.000008	0.282401	0.000022	−13.12	−10.42	1200	1844	−0.97
DSC-11-12	127.2	0.064818	0.001265	0.000932	0.000016	0.282490	0.000021	−9.96	−7.25	1075	1644	−0.97
DSC-11-13	127.9	0.068897	0.001266	0.001014	0.000019	0.282496	0.000021	−9.76	−7.04	1069	1631	−0.97
DSC-11-14	127.6	0.063643	0.000092	0.000971	0.000002	0.282508	0.000024	−9.33	−6.61	1051	1604	−0.97
DSC-11-16	127.0	0.067715	0.000547	0.001030	0.000005	0.282428	0.000022	−12.16	−9.46	1165	1783	−0.97
DSC-11-17	126.3	0.071273	0.000228	0.001205	0.000002	0.282462	0.000024	−10.98	−8.31	1123	1710	−0.96
DSC-11-18	126.9	0.063111	0.000816	0.001001	0.000011	0.282506	0.000021	−9.40	−6.70	1054	1608	−0.97
DSC-11-19	127.7	0.053536	0.000435	0.000971	0.000008	0.282563	0.000021	−7.38	−4.66	973	1480	−0.97
DSC-11-20	128.6	0.082249	0.001025	0.001376	0.000017	0.282569	0.000021	−7.18	−4.48	976	1469	−0.96
HSQ-5-1	126.4	0.053038	0.000352	0.000856	0.000007	0.282564	0.000014	−7.35	−4.64	969	1478	−0.97
HSQ-5-2	126.6	0.069150	0.000833	0.001130	0.000015	0.282555	0.000017	−7.67	−4.99	989	1500	−0.97
HSQ-5-3	126.2	0.081105	0.000823	0.001309	0.000018	0.282552	0.000020	−7.79	−5.13	999	1509	−0.96
HSQ-5-4	125.7	0.051869	0.000819	0.000845	0.000015	0.282570	0.000017	−7.13	−4.45	960	1465	−0.97
HSQ-5-5	125.8	0.090218	0.000654	0.001632	0.000013	0.282572	0.000018	−7.08	−4.46	979	1465	−0.95
HSQ-5-6	125.8	0.053427	0.000121	0.000839	0.000003	0.282608	0.000019	−5.81	−3.12	908	1380	−0.97
HSQ-5-7	128.3	0.045712	0.000281	0.000738	0.000005	0.282511	0.000020	−9.22	−6.47	1040	1595	−0.98
HSQ-5-8	127.0	0.051382	0.000128	0.000820	0.000004	0.282532	0.000021	−8.47	−5.76	1013	1549	−0.98
HSQ-5-9	127.2	0.101513	0.001034	0.002061	0.000029	0.282590	0.000024	−6.45	−3.83	964	1426	−0.94
HSQ-5-10	125.9	0.066626	0.000364	0.001026	0.000010	0.282594	0.000022	−6.30	−3.62	932	1413	−0.97
HSQ-5-11	126.3	0.056580	0.000196	0.000919	0.000003	0.282566	0.000020	−7.27	−4.58	968	1473	−0.97
HSQ-5-13	125.9	0.057929	0.000580	0.001032	0.000007	0.282557	0.000019	−7.59	−4.92	983	1495	−0.97
HSQ-5-14	126.5	0.047506	0.000711	0.000847	0.000014	0.282551	0.000020	−7.80	−5.10	987	1507	−0.97
HSQ-5-15	126.6	0.060705	0.000486	0.001089	0.000009	0.282564	0.000016	−7.34	−4.66	975	1479	−0.97
HSQ-5-16	125.9	0.027131	0.000248	0.000485	0.000004	0.281637	0.000020	−40.15	−37.43	2231	3535	−0.99
HSQ-5-17	125.1	0.093646	0.003929	0.001609	0.000068	0.282610	0.000020	−5.75	−3.13	924	1381	−0.95
HSQ-5-18	126.2	0.048050	0.000243	0.000797	0.000005	0.282557	0.000020	−7.61	−4.91	978	1495	−0.98

Table 2 Continued

Sample	t (Ma)	$^{176}Yb/^{177}Hf$	2σ	$^{176}Lu/^{177}Hf$	2σ	$^{176}Hf/^{177}Hf$	2σ	$\varepsilon_{Hf}(0)$	$\varepsilon_{Hf}(t)(‰)$	T_{DM1} (Ma)	T_{DM2} (Ma)	$f_{Lu/Hf}$
HSQ-5-19	127.3	0.069928	0.000458	0.001289	0.000016	0.282596	0.000018	−6.23	−3.55	935	1409	−0.96
HSQ-5-20	126.9	0.062552	0.000561	0.001024	0.000011	0.282544	0.000020	−8.08	−5.38	1002	1525	−0.97

$\varepsilon_{Hf}(0)=((^{176}Hf/^{177}Hf)_S/(^{176}Hf/^{177}Hf)_{CHUR, 0}-1)\times10000$,

$\varepsilon_{Hf}(t)=((^{176}Hf/^{177}Hf)_S-(^{176}Lu/^{177}Hf)_S\times(e^{\lambda t}-1))/((^{176}Hf/^{177}Hf)_{CHUR,0}-(^{176}Lu/^{177}Hf)_{CHUR}\times(e^{\lambda t}-1))-1)\times10000$,

$T_{DM1}=1/\lambda\times\ln\{1+[(^{176}Hf/^{177}Hf)_S-(^{176}Hf/^{177}Hf)_{DM}]/[(^{176}Lu/^{177}Hf)_S-(^{176}Lu/^{177}Hf)_{DM}]\}$,

$T_{DM2}=T_{DM1}-(T_{DM1}-t)\times((f_{CC}-f_S)/(f_{CC}-f_{DM}))$,

$f_S=(^{176}Lu/^{177}Hf)_S/(^{176}Lu/^{177}Hf)_{CHUR}-1, f_{CC}=(^{176}Lu/^{177}Hf)_C/(^{176}Lu/^{177}Hf)_{CHUR}-1, f_{DM}=(^{176}Lu/^{177}Hf)_{DM}/(^{176}Lu/^{177}Hf)_{CHUR}-1$,

$(^{176}Lu/^{177}Hf)_S$ and $(^{176}Hf/^{177}Hf)_S$ are test values, $(^{176}Lu/^{177}Hf)_{CHUR}=0.03321, (^{176}Hf/^{177}Hf)_{CHUR,0}=0.282772, (^{176}Lu/^{177}Hf)_{DM}=0.03842, (^{176}Hf^{177}Hf)_{DM}=0.28325$

(Blichert-Toft and Albarede, 1997), $(^{176}Lu/^{177}Hf)_C=0.015$ (Griffin et al., 2002), t is the formation time of the sample, $\lambda_{Lu}=1.867\times10^{-11}$ year^{-1} (Soderlund et al., 2004).
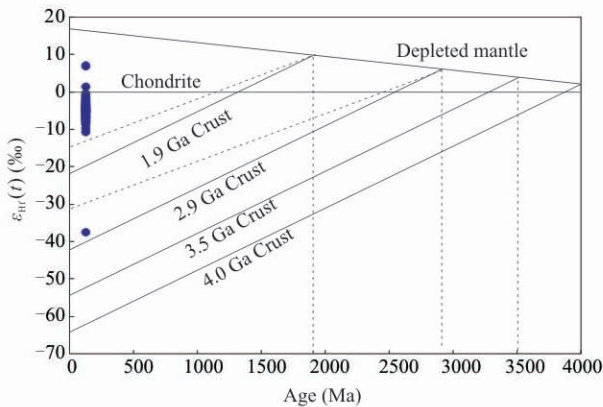
Fig. 8. Hf isotope evolution diagram of zircon of intrusions.

The DM line denotes the evolution of the depleted mantle with a present-day $^{176}Hf/^{177}Hf=0.28325$ and $^{176}Lu/^{177}Hf=0.0384$ (Griffin et al., 2004).The corresponding solid lines of 1.9Ga, 2.9Ga, 3.5Ga and 4.0Ga lower crust evolution in the Liantu and Kongling Formation, which represent the peak ages of crust growth of Yangtze Craton, are calculated by assuming the $^{176}Lu/^{177}Hf$ ratio of 0.009 for average continental crust from the Yangtze Craton (Zhang et al., 2006, Zhang and Zheng, 2007). The dashed lines were drawn assuming that crust growth occurred respectively at continental crust at 1.9Ga and 2.9Ga with $^{176}Lu/^{177}Hf$ ratio of 0.015 for average continental crust (Griffin et al., 2002).

rock stocks (i.e. the distribution of zircons) are above the evolution line of the crust in the Yangtze Craton (Zhang et al., 2006; Zhang and Zheng, 2007) in the intermediate zone connecting the chondrite line to the crustal curve (1.9
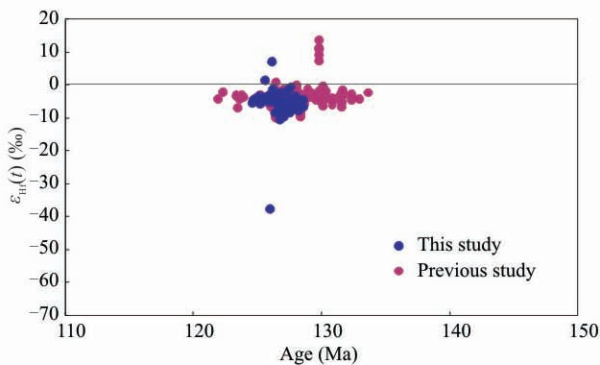
Fig. 9. Plot of the zircon Hf isotopes vs. zircon U-Pb ages for volcanic-subvolcanic rocks and intrusions in Ningwu ore district.

Data are from this study, Hou and Yuan (2010) and Yuan et al. (2011). The zircon Hf isotopes of lower crust are from Kongling metamorphic rocks in the Yangtze Craton (Zhang et al., 2006).

Ga). In addition, there is one zircon grain with much lower $\varepsilon_{Hf}(t)$ value (−37.43) and higher T_{DM2} age (3535 Ma), which is similar to those of the initial stage of the Yangtze craton (Zhang et al., 2006), and two zircon grains with higher $\varepsilon_{Hf}(t)$ values (1.55 and 7.17) and lower T_{DM2} ages (1083 Ma and 724 Ma) are consistent with the higher $\varepsilon_{Hf}(t)$ values (7.64 to 13.91) and younger T_{DM2} (294 Ma to 581 Ma) of the five grain zircons from the samples of the Gushan intrusion obtained by Yuan et al. (2011). The observation also indicates that the granodioritic stocks will not have only one end member source. Furthermore, Münker et al. (2004) and Hanyu et al. (2002) conformed that the Hf element as high-field strength element can affect the composition of the rock by slab melts that originate from subducted oceanic crust. Nebel et al. (2011) presented that $^{176}Hf/^{177}Hf$ decreases from 0.28314 to 0.28268 in the Banda arc, East Indonesia, with an increasing in the involvement of subducted crustal material in the magma source. The Hf isotopic data gained in this study have similar compositions to the end member of involved more crustal signatures. The evidence above reflects dynamic geological evolution which strongly suggests that the source of the rocks was not formed only from one single component end member, and crust material had been assimilated into the source magma generation during its ascent. By reviewing previous studies, one can see that almost all of the Hf isotopic compositions of granodioritic stocks are concordant with those of volcanic rocks and diorite porphyrite (associated with iron ore deposits) in the Ningwu basin with the $\varepsilon_{Hf}(t)$ values concentrated in a range of −1‰ to −9‰ (Fig. 9). Combined with previous studies on Nd-Sr-Pb isotopic characteristics (Xing, 1996; Xing and Xu, 1999; Wang et al., 2001a; Hou et al., 2010; Yuan et al. 2011), we therefore consider that granodioritic stocks might share a similar source with volcanic rocks and diorite porphyrite. Granodioritic rocks occurred in the Ningwu ore district have a close original relationship with dioritic rocks.

5.3 Geodynamic background

It is generally accepted that the magmatism and mineralization in the MLYRB, occurring during the Mesozoic (145–120Ma), has two major episodes: (1) 156–

137 Ma high-K calc-alkaline granitoids associated with 148–135 Ma porphyry-skarn-stratabound Cu-Au-Mo-Fe deposits; (2) 135–123 Ma shoshonitic series associated with 135–123 Ma magnetite-apatite deposits and other small-scale economic deposits (Cu, Au, Pb-Zn) (Chang et al., 1991; Zhai et al., 1992a; Mao et al., 2006, 2009, 2011; Pan and Dong, 1999; NRG, 1978; Ren et al., 1991; Zhou et al., 2008a, 2010). And A-type granitoids (126.5–124.8 Ma) are associated with Au and U mineralization, occurring on the two sides of the lower reaches of Yangtze River (Zhang et al., 1988; Tang et al., 1998; Xing and Xu, 1999; Fan et al., 2008). During that period of time, the tectonic regime underwent significant shift, with the main structural pattern converted from nearly E-W to NE-NNE (Tao et al., 1998; Qi et al., 2000; Dong et al., 2007), possibly experiencing crust thickening, delamination of the lower crust, extension of the tectonic regime, lithospheric thinning, asthenosphere upwelling and crust-mantle interaction (Mao et al., 2005, 2011; Li, 2010a, b; Zhou et al., 2008a; Xie et al., 2006a; Lü et al., 2004; Wang et al., 2001a, b, 2003; Zhang et al., 2001). It is commonly considered that these tectonizations are associated with oblique subduction of the Izanagi plate, which tore up the low-angle subducted slab and the overlying crust along the ore belt due to disharmonious movement of the Yangtze craton and the North China craton beside it (Mao et al., 2011; Zhu et al., 2003, 2010; Sun et al., 2007; Li, 2000; Deng et al., 1992; Qiu et al., 1981).

In the second episode, the geochron of volcanic-subvolcanic rocks and intrusions is concentrated in 135–125 Ma, belonging to the Early Cretaceous, in the MLYRB, mainly including the Ningwu basin (135–126Ma, Zhang et al., 2003; Hou and Yuan, 2010; Xue et al., 2010; Fan et al., 2010; Zhou et al., 2011; Yuan et al., 2011), the Luzong basin (135–127Ma, Zhou et al., 2008b, 2010; Xue et al., 2010; Qin et al., 2010; Zeng et al., 2010), the Jinniu basin (130–125Ma, Xie et al., 2006b, 2011), and the Fanchang basin (134–128Ma, Lou and Du, 2006; Yu and Xu, 2009; Yan et al., 2009; Yuan et al., 2010). We present that the age of iron mineralization in the Ningwu ore district also varies in a narrow range of 131–127 Ma, being consistent with that of the earlier volcanic activity (the Dawangshan Formation). When the oblique subduction of the Izanagi plate transformed its moving direction to NE-NNE and tore up the low-angle subducted slab (Mao et al., 2008, 2011; Zhou et al., 2008a, 2011; Xie et al., 2006b, 2008a, 2008b; Yuan et al., 2008; Xing and Xu, 1999). Based on geochemical and geochronological studies, Xie et al. (2011), Yuan et al. (2008, 2010) and Yan et al. (2009) suggested that volcanic rocks in the Fanchang basin, Jinniu basin and part of the Luzong basin are characterized by bimodal volcanic rocks, occurring in

the same period. Besides, A-type granite occurred partially and transitorily during 126.5–124.8 Ma (Fan et al., 2008), slightly later than iron mineralization in the MLYRB. The above discussion provides evidence that Early Cretaceous volcanic rocks and the porphyry iron mineralization in the MLYRB were developed in an extensional tectonic regime induced by the Izanagi plate while transforming its moving direction to NE-NNE and the low-angle subducted slab tearing up (Mao et al., 2005, 2008, 2011; Zhou et al., 2008a; Xie et al., 2011), and the previous subducted slab remaining in the asthenosphere might have contributed to the rock-forming process. Magmatism and mineralization of porphyry iron deposits in the Ningwu ore district occurred also in an extensional tectonic regime.

6 Conclusions

Based on the above analyses and discussion, the following conclusions can be reached:

(1) Emplacement and crystallization (typically for zircons) of the granodioritic stocks in the study area occurred at an age range of 126–127 Ma, and the age of the iron mineralization in the Ningwu ore district is in a very short period of 131–127 Ma.

(2) Granodioritic rocks occurring in the Ningwu ore district have a close original relationship with dioritic rocks.

(3) Magmatism and mineralization of porphyry iron deposits in the Ningwu ore district occurred in an extensional tectonic regime induced as the Izanagi plate transformed its moving direction to NE-NNE.

References

Amelin, Y., Lee, D.C., Halliday, A.N., and Pidgeon, R.T., 1999. Nature of the Earth's earliest crust from hafnium isotopes in single detrital zircons. *Nature*, 399: 252–255.

Belousova, E.A., Griffin, W.L., O'Reilly, S.Y., and Fisher, N.I., 2002. Igneous zircon: trace element composition as an indicator of source rock type. *Contributions to Mineralogy and Petrology*, 143(5): 602–622.

Blichert-Toft, J., and Albarede, F., 1997. The Lu-Hf isotope geochemistry of chondrites and the evolution of the mantle-crust system. *Earth and Planetary Science Letters*, 148: 243–258.

Chang Yinfo, Liu Xiangpei and Wu Yanchang, 1991. *The Copper-Iron Belt of the Lower and Middle Reaches of the Changjiang River*. Beijing: Geological Publishing House, 379 (in Chinese with English abstract).

Chauvel, C., and Blichert-Toft, J., 2001. A hafnium isotope and trace element perspective on melting of the depleted mantle. *Earth and Planetary Science Letters*, 190: 137–151.

Chu, N.C., Taylor, R.N., Chavagnac, V., Nesbitt, R.W., Boella, R.M., Milton, J.A., German, C.R., Bayon, G., and Burton, K., 2002. Hf isotope ratio analysis using multi-collector inductively coupled plasma mass spectrometry: an evaluation of isobaric interference corrections. *J. Anal. At. Spectrom.*, 17: 1567–1574.

Deng Jinfu, Ye Delong, Zhao Hailing and Tang Haiping, 1992.*Volcanism, deep internal processes and basin formation in the Lower Reaches of Yangtze River*. Wuhan: China University of Geosciences Press, 184 (in Chinese with English abstract).

Dong Shuwen, Zhang Yueqiao, Long Changxing, Yang Zhenyu, Ji Qiang, Wang Tao, Hu Jianmin and Chen Xuanhua, 2007. Jurassic tectonic revolution in China and new interpretation of the Yanshan movement. *Acta Geologica Sinica*, 81(11): 1449–1461 (in Chinese with English abstract).

Fan Yu, Zhou Taofa, Yuan Feng, Qian Cunchao, Lu Sanming and Cooke, D.R., 2008. LA-ICP-MS zircon U-Pb ages of the A-type granites in the Lu-Zong (Lujiang-Zongyang) area and their geological significances. *Acta Petrologica Sinica*, 24(8): 1715–1724 (in Chinese with English abstract).

Fan Yu, Zhou Taofa, Yuan Feng, Zhang Lejun, Qian Bin, Ma Liang and Cooke, D.R., 2010. Geochronology of the diorite porphyrites in Ning-Wu basin and their metallogenic significances. *Acta Petrologica Sinica*, 26(9): 2715–2728 (in Chinese with English abstract).

Griffin, W.L., Wang, X., Jackson, S.E., Pearson, N.J., and O'Reilly, S.Y., 2002. Zircon geochemistry and magma mixing, SE China: in situ analysis of Hf isotopes, Tonglu and Pingtan igneous complexes. *Lithos*, 61: 237–269.

Griffin, W.L., Belousova, E.A., Shee, S.R., Pearson, N.J., and O'Reilly, S.Y., 2004. Archean crustal evolution in the northern Yilgarn Craton: U-Pb and Hf-isotope evidence from detrital zircons. *Precambrian Research*, 131: 231–282.

Hamelin, C., Dosso, L., Hanan, B., and Barrat, J.A., 2010. Sr-Nd-Hf isotopes along the Pacific Antarctic Ridge from 41 to 53° S. *Geophysical Research Letters*, 37: L10303, doi: 10.1029/2010GL042979.

Hanyu, T., Tatsumi, Y., and Nakai, S., 2002. A contribution of slab-melts to the formation of high-Mg andesite magmas; Hf isotopic evidence from SW Japan. *Geophysical Research Letters*, 29(22): 2051, doi:10.1029/2002GL015856.

Hoskin, P.W.O., and Black, L.P., 2000. Metamorphic zircon formation by solid-state recrystallization of protolith igneous zircon. *Journal of Metamorphic Geology*, 18(4): 423–439.

Hou, K.J., Li, Y.H., Zou, T.R., Qu, X.M., Shi, Y.R., and Xie, G.Q., 2007. Laser ablation-MC-ICP-MS technique for Hf isotope microanalysis of zircon and its geological applications. *Acta Petrologica Sinica*, 23(10): 2595–2604 (in Chinese with English abstract).

Hou Kejun, Li Yanhe and Tian Yourong, 2009. In situ U-Pb zircon dating using laser ablation-multi ion couting-ICP-MS. *Mineral Deposits*, 28(4): 481–492 (in Chinese with English abstract).

Hou Kejun and Yuan Shunda, 2010. Zircon U-Pb age and Hf isotopic composition of the volcanic and sub-volcanic rocks in the Ningwu basin and their geological implications. *Acta Petrologica Sinica*, 26(3): 888–902 (in Chinese with English abstract).

Hou, T., Zhang, Z.C., Encarnacion, J., Du, Y.S., Zhao, Z.D., and Liu, J.L., 2010. Geochemistry of Late Mesozoic dioritic porphyries associated with Kiruna-style and stratabound carbonate-hosted Zhonggu iron ores, Middle–Lower Yangtze Valley, Eastern China: Constraints on petrogenesis and iron sources. *Lithos*, 119: 330–344.

IGCAS (Institute of Geochemistry, China Academy of Sciences), 1987. *Ore-forming Mechanism of Ningwu type iron deposits*. Beijing: Science Press, 152 (in Chinese).

Jackson, S.E., Pearson, N.J., Griffin, W.L., and Belousova, E., 2004. The application of laser ablation inductively coupled plasma mass spectrometry to in-situ U–Pb zircon geochronology. *Chemical Geology*, 211: 47–69.

Li, J.W., Deng, X.D., Zhou, M.F., Liu, Y.S., Zhao, X.F., and Guo, J.L., 2010a. Laser ablation ICP-MS titanite U-Th-Pb dating of hydrothermal ore deposits: A case study of the Tonglushan Cu-Fe-Au skarn deposit, SE Hubei Province, China. *Chemical Geology*, 270: 56–67.

Li, X.H., 2000. Cretaceous magmatism and lithospheric extension in Southeast China. *Journal of Asian Earth Sciences*, 18(3): 293–305.

Li, X.H., Li, W.X., Wang, X.C., Li, Q.L., Liu, Y., Tang, G.Q., Gao, Y.Y., and Wu, F.Y., 2010b. SIMS U-Pb zircon geochronology of porphyry Cu-Au-(Mo) deposits in the Yangtze River Metallogenic Belt, eastern China: Magmatic response to early Cretaceous Lithospheric extension. *Lithos*, 119: 427–438.

Liu, Y.S., Hu, Z.C., Gao, S., Gunther, D., Xu, J., Gao, C., and Chen, H., 2008. In situ analysis of major and trace elements of anhydrous minerals by LA-ICP-MS without applying an internal standard. *Chemical Geology*, 257: 34–43.

Lou, Y.E., and Du, Y.S., 2006. Characteristics and zircon SHRIMP U-Pb ages of the Mesozoic intrusive rocks in Fanchang, Anhui Province. *Geochemica*, 35(4): 359–366 (in Chinese with English abstract).

Lü Qingtian, Hou Zengqian, Yang Zhusen and Shi Danian, 2004. Upplating process and dynamics evolution mode in the Middle and Low Reach of Yangtze River: Constraint of physical geography information. *Science in China* (Series D), 34(9): 784–794 (in Chinese).

Ma Fang, Jiang Shaoyong, Jiang Yaohui, Wang Rucheng, Lin Hongfei and Ni Pei, 2006. Pb isotope research of porphyrite Fe Deposits in the Ning-Wu Area. *Acta Geologica Sinica*, 80 (2): 279–286 (in Chinese with English abstract).

Ma Fang, Jiang Shaoyong and Xue Huaimin, 2010. Early Cretaceous mineralications in Mingwu basin: Insight from actinolite ^{39}Ar-^{40}Ar laser dating results. *Mineral Deposits*, 29 (2): 283–289 (in Chinese with English abstract).

Mao Jingwen, Xie Guiqing, Zhang Zuoheng, Li Xiaofeng., Wang Yitian, Zhang Changqing and Li Yongfeng, 2005. Mesozoic large-scale metallogenic pulses in North China and Corresponding geodynamic setting. *Acta Petrologica Sinica*, 21(1): 169–188 (in Chinese with English abstract).

Mao, J.W., Wang, Y.T., Lehmann, B., Yu, J.J., Du, A.D., Mei, Y.X., Li, Y.F., Zang, W.S., Stein, H .J., and Zhou, T.F., 2006. Molybdenite Re-Os and albite ^{40}Ar/^{39}Ar dating of Cu-Au-Mo and magnetite porphyry systems in the Yangtze River valley and metallogenic implications. *Ore Geology Reviews*, 29 (3–4): 307–324.

Mao J.W., Chen Y.C., and Yu J.J., 2008. The iron oxide-apatite deposits in the Ningwu Cretaceous basin in the Lower Reach of the Yangtze River valley, China. *The 33rd IGC international geological congress*, Oslo, abstract.

Mao Jingwen, Shao Yongjun, Xie Guiqing, Zhang Jiandong and Chen Yuchuan, 2009. Mineral deposit model for porphyry-skarn polymetallic copper deposits in Tongling ore dense district of Middle-Lower Yangtze Valley metallogenic belt. *Mineral Deposit*s, 28(2): 109–119 (in Chinese with English abstract).

Mao, J.W., Xie, G.Q., Duan, C., Pirajno, F., Ishiyama, D., and Chen, Y.C., 2011. A tectono-genetic model for porphyry-skarn Cu-Au-Mo-Fe and magnetite-apatite deposits along Middle-Lower Yangtze River Valley, Eastern China. *Ore Geology Reviews*. 43(1): 294–314.

Morel, M.L.A., Nebel, O., Nebel-Jacobsen, Y.J., Miller, J.S., and Vroon, P.Z., 2008. Hafnium isotope characterization of the GJ-1 zircon reference material by solution and laser-ablation MC-ICPMS. *Chemical Geology*, 255: 231–235.

Münker, C., Wörner, G., Yogodzinski, G.M., and Churikova, T.G., 2004. Behaviour of high field strength elements in subduction zones: constraints from Kamtchatka–Aleutian arc lavas. *Earth and Planetary Science Letters*, 224: 275–293.

Nasdala, L., Hofmeister, W., Norberg, N., Mattinson, J.M., Corfu, F., Dorr, W., Kamo, S.L., Kennedy, A.K., Kronz, A., Reiners, P.W., Frei, D., Kosler, J., Wan, Y.S., Gotze, J., Hager, T., Kroner, A., and Valley, J.W., 2008. Zircon M257 - a homogeneous natural reference material for the ion microprobe U-Pb analysis of zircon. *Geostandards and Geoanalytical Research*, 32(3): 247–265.

Nebel, O., Vroon, P.Z., van Westrenen, W., Iizuka, T., and Davies, G.R., 2011. The effect of sediment recycling in subduction zones on the Hf isotope character of new arc crust, Banda arc, Indonesia. *Earth and Planetary Science Letters*, 303: 240–250.

NRG (Ningwu Research Group), 1978. *Magnetite Porphyry Deposits in Ningwu Area*. Beijing: Geological Publishing House, 196 (in Chinese).

Pan, Y.M., and Dong, P., 1999. The Lower Changjiang (Yangzi/ Yangtze River) metallogenic belt, East China: Intrusion- and wall rock-hosted Cu-Fe-Au, Mo, Zn, Pb, Ag deposits. *Ore Geology Reviews*, 15(4): 177–242.

Patchett, P.J., and Tatsumoto, M., 1980. Hafnium isotope variation in oceanic basalts, *Geophys. Res. Lett.*, 7: 1077–1080.

Patchett, P.J., 1983. Hafnium isotope results from mid-ocean

ridges and Kerguelen. *Lithos*, 16: 47–51.

Qi Jianzhong, Liu Hongying and Jiang Yaohui, 2000. Yenshanian subduction and strike-sliping regime of East China, and its control of ore localization. *Volcanology and Mineral Resources*, 21(4): 244–265 (in Chinese with English abstract).

Qin, Y.J., Zeng, J.N., Ma, Z.D., Chen, J.H., and Jin, X., 2010. Zircon LA-ICP-MS U-Pb dating of ore-bearing pyroxene-trachyandesite porphyry and its geological significance in Luohe-Nihe iron ore field in Luzong basin, southern Anhui, China. *Geological Bulletin of China*, 29(6): 851–862.

Qiu Jiaxiang, Wang Renjing, Wang Fangzheng and Li Changnian, 1981. The petrochemical characteristics and petrogenetic analysis of Mesozoic volcanics along the Lower Reaches of Yangtze River. *Earth Science*, 6(1): 170–182 (in Chinese with English abstract).

Ren Qijiang, Liu Xiaoshan, Xu Zhaowen, Qiu Detong, Hu Wenxuan, Fang Changqiao, Ruan Huichu, Dong Huogen, Li Zhaolin and Wu Qizhi, 1991. *Mesozoic volcano-tectonic depression and its mineralizing process in Lujiang-Zongyang area, Anhui Province*. Beijing: Geological Publishing House, 206 (in Chinese with English abstract).

Salters, V.J.M., and Hart, S.R., 1991. The mantle sources of ocean ridges, islands and arcs: the Hf-isotope connection. *Earth and Planetary Science Letters*, 104: 364–380.

Salters, V.J.M., 1996. The generation of mid-ocean ridge basalts from the Hf and Nd isotope perspective. *Earth and Planetary Science Letters*, 141: 109–123.

Salters, V.J.M., and White, W.M., 1998. Hf isotope constraints on mantle evolution. *Chemical Geology*, 145: 447–460.

Siebel, W., and Chen, F.K., 2010. Zircon Hf isotope perspective on the origin of granitic rocks from eastern Bavaria, SW Bohemian Massif. *International Journal of Earth Sciences*, 99: 993–1005.

Sláma, J., Kosler, J., Condon, D.J., Crowley, J.L., Gerdes, A., Hanchar, J.M., Horstwood, M.S.A., Morris, G.A., Nasdala, L., Norberg, N., Schaltegger, U., Schoene, B., Tubrett, M.N., and Whitehouse, M.J., 2008. Plesovice zircon — A new natural reference material for U-Pb and Hf isotopic microanalysis. *Chemical Geology*, 249: 1–35.

Soderlund, U., Patchett, P.J., Vervoort, J.D., and Isachsen, C.E., 2004. The ^{176}Lu decay constant determined by Lu-Hf and U-Pb isotope systematics of Precambrian mafic intrusions. *Earth and Planetary Science Letters*, 219: 311–324.

Sun, W.D., Ding, X., Hu, Y.H., and Li, X.H., 2007. The goldeng transformation of the Cretaceous plate subduction in the west Pacific. *Earth and Planet Science Letter*, 262(3–4): 533–542.

Tang Yongcheng, Wu Yanchang, Chu Guozheng, Xing Fengming, Wang Yongmin, Cao Fenyang and Chang Yinfo, 1998. *Geology of copper-gold polymetallic deposits in the along-Changjiang area of Anhui Province*. Beijing: Geological Publishing House, 351 (in Chinese with English abstract).

Tao Kuiyuan, Mao Jianren, Yang Zhuliang, Zhao Yu, Xing Guangfu and Xue Huaimin, 1998. Mesozoic petro-tectonic associations and records of the geodynamic processes in Southeast China. *Earth Science Frontiers*, 5(4): 183–190 (in Chinese with English abstract).

Tu Wei, Du Yangsong, Li Shunting and Gao Zhiwei, 2010. Petrographic and mineralogica characteristics of Jiangmiao olivine gabbros in the Ningwu basion and it implication for

tectonics. *Journal of Mineralogy and Petrology*, 30(1): 47–52 (in Chinese with English abstract).

Wang Qiang, Zhao Zhenhua, Xiong Xiaolin and Xu Jifeng, 2001b. Melting of the underplated basaltic lower crust: Evidence from the Shaxi adakitic sodic quartz diorite-porphyrites, Anhui Province, China. *Geochimica*, 30 (4): 353–362 (in Chinese with English abstract).

Wang Qiang, Xu Jifeng, Zhao Zhenhua, Xiong Xiaolin and Bao Zhiwei, 2003. Petrogenesis of the Mesozoic intrusive rocks in the Tongling area, Anhui Province, China and their constraint on geodynamic process. *Science in China* (Series D), 33(4): 323–334 (in Chinese).

Wang, X., Griffin, W. L., Chen, J., Huang, P., and Li, X., 2011. U and Th Contents and Th/U Ratios of Zircon in Felsic and Mafic Magmatic Rocks: Improved Zircon-Melt Distribution Coefficients. *Acta Geologica Sinica* (English Edition), 85(1): 164–174.

Wang Yuanlong, Zhang Qi and Wang Yan. 2001a. Geochemical characteristics of volcanic rocks from Ningwu area, and its significance. *Acta Petrologica Sinica*, 17(4): 565–575 (in Chinese with English abstract).

Wu, F.Y., Yang, Y.H., Xie, L.W., Yang, J.H., and Xu, P., 2006. Hf isotopic compositions of the standard zircons and baddeleyites used in U–Pb geochronology. *Chemical Geology*, 234: 105–126.

Wu, F.Y., Li, X.H., Zheng, Y.F., and Gao, S., 2007. Lu-Hf isotopic systematics and their applications in petrology. *Acta Petrologica Sinica* 23: 185–220 (in Chinese with English abstract).

Xie Guiqing, Mao Jingwen, Li Ruiling, Zhang Zusong, Zhao Weichao, Qu Wenjun, Zhao Caisheng and Wei Shikun, 2006a. Metallogenic epoch and geodynamic frame work of Cu-Au-Mo-(W) deposits in Southeastern Hubei Province: Constraints from Re-Os molybdenite ages. *Mineral Deposits*, 25(1): 43–52 (in Chinese with English abstract).

Xie Guiqing, Mao Jingwen, Li Ruiling, Zhou Shaodong, Ye Huishou, Yan Quanren and Zhang Zusong, 2006b. SHRIMP zircon U-Pb dating for Volcanic rocks of the Dasi Formation in Southeast Hubei Province, Middle-Lower Reaches of the Yangtze River and its implications. *Chinese Science Bulletin*, 51(24): 3000–3009.

Xie, G.Q., Mao, J.W., Li, R.L., and Bierlein, F.P., 2008a. Geochemistry and Nd–Sr isotopic studies of Late Mesozoic granitoids in the southeastern Hubei Province, Middle–Lower Yangtze River belt, Eastern China: Petrogenesis and tectonic setting. *Lithos*, 104(1–4): 216–230.

Xie Guiqing, Li Ruiling, Jiang Guohao, Zhao Caisheng and Hou Kejun, 2008b. Geochemistry and petrogenesis of late Mesozoic granitoids in southeastern Hubei Province and constrains on the timing of lithospheric thinning, Middle-Lower Reaches of the Yangtze River, eastern China. *Acta Petrologica Snica*, 24(8): 1703–1714 (in Chinese with English abstract).

Xie, G.Q., Mao, J.W., Li, X.W., Duan, C., and Yao, L., 2011. Late Mesozoic bimodal volcanic rocks in the Jinniu basin, Southeast Hubei Province, Middle–Lower Yangtze River Belt (MLYRB), East China: age, petrogenesis and tectonic implication. *Lithos* , 127: 144–146.

Xing, F.M., 1996. Petrological and Nd, Sr, Pb isotopic evidence for genesis of Mesozoic magmatic rocks in Nanjing–Wuhu area. *Acta Petrologica et Mineralogica*, 15: 126–137 (in Chinese with English Abstract)

Xing Fengming and Xu Xiang, 1999. *Magmatic belt and mineralization in Yangtze River Reaches of Anhui Province*. Hefei: Anhui People Publication House, 1–170 (in Chinese).

Xue Huaimin, Dong Shuwen and Ma Fang, 2010. Zircon U-Pb SHRIMP ages of sub-volcanic bodies related with porphyritic Fe-deposits in the Luzong and Ningwu basins, Middle and Lower Yangtze River Reaches, Central China. *Acta Petrologica Sinica*, 26(9): 2653–2664 (in Chinese with English abstract).

Yan, J., Liu, H.Q., Song, C.Z., Xu, X.S., An, Y.J., Liu, J., and Dai, L.Q., 2009. Zircon U-Pb geochronology of the volcanic rocks from Fangchang-Ningwu volcanic basins in the Lower Yangtze region and its geological implications. *Chinese Science Bulletin*, 54(16): 2895–2904.

Yu Jinjie and Mao Jingwen, 2002. Rare earth elements in apatite from porphyrite iron deposits of Ningwu area. *Mineral Deposits*, 21(1): 65–73 (in Chinese with English abstract).

Yu, J.J., and Mao, J.W., 2004. ^{40}Ar/^{39}Ar dating of albite and phlogopite from porphyry iron deposits in the Ningwu basin in east-central China and its significance. *Acta Geologica Sinica* (English edition), 78(2): 435–422.

Yu, J.J., Zhang, Q., Mao, J.W., and Yan, S.H., 2007. Geochemistry of apatite from the apatite-rich iron deposits in the Ningwu Region, East Central China. *Acta Geologica Sinica* (English edition),, 81(4): 637–648.

Yu, J.J., Mao, J.W., and Zhang, C.Q., 2008. The possible contribution of a mantle-derived fluid to the Ningwu porphyry iron deposits-Evidence from carbon and strontium isotopes of apatites. *Progress in Natural Science*, 18(2): 167–172.

Yu, Y., and Xu, X.S., 2009. Cretaceous alkali-rich magmatism in the Middle and Lower Reaches of the Yangtze River. *Earth Science Journal of China University of Geosciences*, 34(1): 105–116 (in Chinese with English abstract).

Yuan Feng, Zhou Taofa, Fan Yu, Lu Sanming, Qian Cunchao, Zhang Lejun, Duan Chao and Tang Minhui, 2008. Source, evolution and tectonic setting of Mesozoic volcanic rocks in Luzong basin, Anhui Province. *Acta Petrologica Sinica*, 24 (8): 1691–1702 (in Chinese with English abstract).

Yuan Feng, Zhou Taofa, Fan Yu, Zhang Lejun, Ma Liang and Qian Bing, 2011. Zircon U-Pb ages and isotopic characteristics of the granitoids in the Ningwu basin, China, and their significance. *Acta Geologica Sinica*, 85(5): 822–834 (in Chinese with English abstract).

Yuan Shunda, Hou Kejun and Liu Min, 2010. Timing of mineralization and geodynamic framework of iron-oxide-apatite deposits in Ningwu Cretaceous basin in the Middle-Lower Reaches of the Yangtze River, China: Constraints from Ar-Ar dating on phlogopites. *Acta Petrologica Sinica*, 26(3): 797–808 (in Chinese with English abstract).

Zeng, J.N., Qin, Y.J., Guo, K.Y., Chen, G.G., and Zeng, Y., 2010. Zircon U-Pb dating of ore-bearing magmatic rocks and its constraint on the formation time of the ore deposits in Luzong Basin, Anhui Province. *Acta Geologica Sinica*, 84(4): 466–478 (in Chinese with English abstract).

Zhai Yusheng, Yao Shuzhen, Lin Xinduo, Zhou Xunruo, Wan Tianfeng, Jin Fuquan and Zhou Zonggui, 1992a. *Fe-Cu-Au Metallogeny of the Middle-Lower Changjiang Region*. Beijing: Geological Publishing House, 235 (in Chinese).

Zhai, Y.S., Yao, S.Z., Lin, X.D., Zhou, X.R., Wan, T.F., and Zhou, Z.G.., 1992b. Metallogenic regularity of iron and

copper deposits in the Middle and Lower Valley of the Yangtze River. *Mineral Deposits*, 11: 1–12 (in Chinese with English abstract).

Zhang Bangtong, Zhang Fusheng, Ni Qisheng, Chen Peirong, Zhai Jianping and Shen Weizhou, 1988. Geology and geochemical characteristics of the Anqing-Lujiang quartz syenite rock belt and its genesis. *Acata Petrologica Sinica*, 4 (3): 1–12 (in Chinese with English abstract).

Zhang Qi, Wang Yan, Qian Qing, Yang Jinhui, Wang Yuanlong, Zhao Taiping and Guo Guangjun, 2001. The characteristics and tectonic-metallogenic significances of the adakites in Yanshan period from eastern China. *Acta Petrologica Sinica*, 17(2): 236–244 (in Chinese with English abstract).

Zhang Qi, Jian Ping, Liu Dunyi, Wang Yuanlong, Qian Qing and Xue Huaimin, 2003. SHRIMP dating of volcanic rocks from Ningwu area and geological implication. *Science in China* (Series D), 33 (4): 830–837 (in Chinese).

Zhang, S.B., Zheng, Y.F., Wu, Y.B., Zhao, Z.F., Gao, S., and Wu, F.Y., 2006. Zircon isotope evidence for ≥3.5 Ga continental crust in the Yangtze craton of China. *Precambrian Research*, 146: 16–34.

Zhang, S.B., and Zheng, Y.F., 2007. Growth and reworking of the Yangtze continental nucleus: evidence from zircon U-Pb ages. *Acta Petrologica Sinica*, 23: 393–402 (in Chinese with English abstract).

Zhou Taofa, Fan Yu and Yuan Feng, 2008a. Advances on petrogenesis and metallogenic study of the mineralization belt of the Middle and Lower Reaches of the Yangtze River area. *Acta Petrologica Sinica*, 24(8): 1665–1678 (in Chinese with English abstract).

Zhou Taofa, Fan Yu, Yuan Feng, Lu Sanming, Shang Shigui, Cooke, D.R., Meffre, S., and Zhao Guochun, 2008b. Geochronology of the volcanic rocks in the Lu-Zong basin and its significance. *Science in China* (Series D), 51(10): 1470–1482.

Zhou Taofa, Fan Yu, Yuan Feng, Song Chuanzhong, Zhang Lejun, Qian Cunchao, Lu Sanming and Cooke, D.R., 2010. Temporal-spatial framework of magmatic intrusions in Luzong volcanic basin in East China and their constrain to mineralization. *Acta Petrologica Sinica*, 26(9): 2694–2714 (in Chinese with English abstract).

Zhou, T.F., Fan, Y., Yuan, F., Zhang, L.J., Qian, B., Ma, L., Yang, X.F., and Cooke, D.R., 2011. Geochronology and significance of volcanic rocks in the Ning-Wu basin of China. *Science in China* (Series D), 54(2): 185–196.

Zhu, G., Niu, M.L., Xie, C.L., and Wang, Y.S., 2010. Sinistral to Normal Faulting along the Tan-Lu Fault Zone: Evidence for Geodynamic Switching of the East China Continental Margin. *The Journal of geology*, 118(3): 277–293.

Zhu Guang, Liu Guosheng Niu Manlan, Song Chuanzhong and Wang Daoxuan, 2003. Transcurrent movement and genesis of the Tan-Lu fault zone. *Geological Bulletin of China*, 22(3): 200–207 (in Chinese with English abstract).